biomimetics

MDPI

Review

Connectomes as Structural Priors for Embodied Control: Lessons from Digital *Drosophila*

Wenxiang Jiang and Lihong Xu *

School of Electronic and Information Engineering, Tongji University, Shanghai 201804, China; jiangwx@tongji.edu.cn
* Correspondence: xulihong@tongji.edu.cn

Abstract

Synapse-resolved connectomes of *Drosophila melanogaster* now map the entire adult brain and ventral nerve cord, but behavior also depends on synaptic strengths, neural dynamics, and the body. A connectome is therefore better used as a testable structural prior than as a blueprint to copy. This review examines how digital *Drosophila* (connectomes plus the models and body simulators built on them) can serve this role in embodied control. We trace how electron-microscopy images become a connectivity graph, where errors enter, and how heterogeneous datasets can be combined reproducibly. We then compare three uses of the graph (extracting a circuit principle, embedding a reconstructed module, or adopting the whole connectome as controller topology) with one another and with conventional controllers, separating experimentally validated findings from computational predictions. Connectome-constrained models can predict neural activity and sensorimotor pathways, but simulated success does not by itself establish biological accuracy, and sensory encoding, motor decoding, and body mechanics are as much part of the controller as the wiring. From this synthesis we derive five candidate design principles (sparse modular communication, recurrent state estimation, hierarchical motor control, selective plasticity, and body–controller co-design) and one methodological principle (anatomically indexed intervention), each paired with falsifiable predictions, matched baselines, and sim-to-real stress tests.

Keywords: *Drosophila*; connectomics; bioinspired technologies; embodied intelligence; sensorimotor control

Check for updates

Academic Editors: Antonio Concilio and Longhui Qin

Received: 13 October 2026
Revised: 11 November 2026
Accepted: 13 November 2026
Published: 16 November 2026

Copyright: © 2026 by the authors. Licensee MDPI, Basel, Switzerland. This article is an open access article distributed under the terms and conditions of the Creative Commons Attribution (CC BY) license.

1. Introduction

Embodied intelligence studies agents whose perception, internal computation, and action are shaped by the body and its interaction with the environment [1,2]. From this perspective, the nervous system is more than an abstract policy: behavior emerges from the interplay of neural circuits, muscles, body mechanics, and sensory feedback [3,4]. Insects are attractive models for this problem because their compact nervous systems support navigation, flight, walking, and learning [5,6] and because their anatomy can now be reconstructed at a resolution that remains difficult to achieve in larger animals. The adult fruit fly, *Drosophila melanogaster*, occupies a useful middle ground. Its brain of roughly 1.4×10^5 neurons [7] and supports a rich sensorimotor repertoire, yet it is small enough to be mapped synapse by synapse and is accessible to an extensive set of genetic and physiological tools [8].

We use the term digital *Drosophila* for an integrated computational representation rather than for a single software package. It comprises volumetric anatomical data, recon-

structed neurons and synapses, cell-type annotations, graph representations of connectivity, neural or dynamical models, and body–environment simulators. The whole-brain electron-microscopy (EM) volume of the Full Adult Fly Brain (FAFB) project, reported by Zheng et al., established a reference for adult *Drosophila* brain reconstruction [9]. Later resources expanded both the scale and the usability of the data: FlyWire provides a community- and machine-assisted reconstruction of the whole adult brain [7,10], and the Brain And Nerve Cord (BANC) project extends coverage to the brain, neck connective, and ventral nerve cord (VNC) of a single female [11]. With these resources in hand, the central question shifts from whether insect wiring can be observed to how wiring can constrain an executable controller [12].

For biomimetic design, the goal is not a literal copy of *Drosophila*. A connectome acts as a structured prior: it indicates which units communicate, which pathways recur, where information converges, and where control may be modularized. By itself, it does not determine synaptic weights, temporal dynamics, neuromodulatory state, muscle recruitment, or the physical consequences of an action [13,14]. This distinction becomes decisive when a biological circuit is transferred to a robot or to a simulated body. The engineering value of a circuit is established by comparing a connectome-constrained model with suitable baselines inside a task-relevant body–environment loop.

This review has four aims. First, it traces the technical chain from tissue preparation and volume EM to a graph that can be queried or simulated, together with practices for combining datasets reproducibly. Second, it distinguishes well-established data products and experimentally validated findings from biological quantities that remain uncertain and from computational predictions. Third, it organizes model-building options by how strongly they impose biological structure on an artificial controller, appraises existing models critically, and compares them with conventional controllers. Fourth, it extracts design principles, stated as falsifiable predictions, that can be tested in other embodied agents, with particular attention to recurrent control, modularity, plasticity, and the interface between a neural graph and a physical body. The emphasis is therefore on transferable mechanisms and evaluation logic rather than on reproducing *Drosophila* behavior in every biological detail.

Scope and literature selection.This is a narrative, critical review rather than a systematic review. Literature was identified through searches of Web of Science, PubMed, Google Scholar, arXiv, and bioRxiv that combined terms for *Drosophila* connectomics (for example, connectome, FlyWire, hemibrain, ventral nerve cord, and electron microscopy) with terms for computational modeling and embodied control (for example, connectome-constrained model, neuromechanical model, and locomotion control), and it was supplemented by backward and forward citation tracking from the principal dataset papers. The emphasis is on work published between 2013 and 2026; earlier studies are included where they define a method or concept. Studies were included when they (i) reported a synapse-resolved *Drosophila* dataset or a method used to produce or query one; (ii) built an executable model whose structure was constrained by such data; (iii) provided a *Drosophila* body model or closed-loop simulator; or (iv) provided an insect-inspired, robotic, or machine-learning result that serves as a comparator or methodological control. Peer-reviewed articles are the default source of evidence. Two preprints are retained because they provide evidence not yet available in peer-reviewed form: the Male Adult Nerve Cord (MANC) connectome, published as an eLife Reviewed Preprint [15], and the FlyGM whole-brain graph policy, an arXiv preprint that has not been peer reviewed [16]. Both are marked with a dagger (†) in the tables, and conclusions that rest on them are described as preliminary.

Figure 1 summarizes this chain, and its upper row reads from left to right. An adult fly (first panel) is fixed, stained, and imaged as a stack of serial EM sections (second panel;

Section 3). Segmentation and synapse assignment turn the image stack into a brain-wide wiring diagram, drawn as reconstructed neurons of the left and right hemispheres joined by synaptic connections (third panel; Sections 3.2 and 3.3). The wiring diagram then constrains an executable neural network in which input units, internal units, and output units are assigned dynamics (fourth panel; Section 4). The network drives an articulated neuromechanical body model, whose joints are highlighted in orange (fifth panel), and the body acts in a simulated environment containing a raised step, stones, and vegetation (sixth panel; Section 5).

The return arrow along the bottom of Figure 1 closes the sensorimotor loop. Its four icons stand for the main classes of feedback that movement generates: mechanosensory and proprioceptive signals (waveform), contact and load forces between the legs and the substrate (arrows pressing on a surface), odor cues (plume lines), and visual input such as optic flow (eye). Current *Drosophila* body simulators expose these channels to a controller [17], and in the animal each is processed by dedicated sensory circuits rather than relayed as a raw measurement [18,19]. The arrow ends at the animal because closed-loop behavior is also where a model is compared with the real fly; a mismatch at this stage can send the modeler back to revise the sensory encoding, the dynamics, or the interpretation of the reconstruction itself.

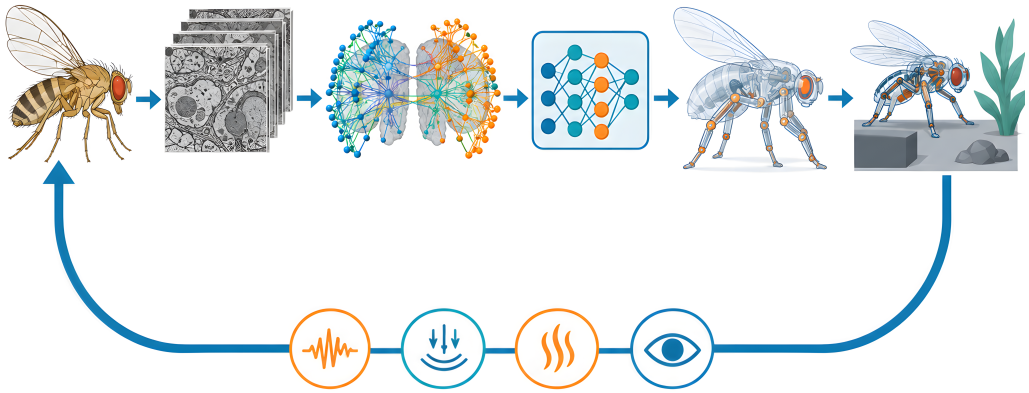


Figure 1. Schematic overview of the chain from reconstructed tissue to embodied control. Upper row, from left to right: the adult fly; serial EM sections; a brain-wide wiring diagram, with reconstructed neurons of the left and right hemispheres in blue and orange and synaptic connections drawn as lines; a connectome-constrained neural network with input, internal, and output units; an articulated neuromechanical body model with actuated joints (orange); and the body acting in a simulated environment. Each arrow marks a transformation that adds modeling assumptions: segmentation and synapse assignment (images to graph), assignment of dynamics and interfaces (graph to network), motor decoding (network to body), and physical simulation (body to environment). Lower return path: the sensory consequences of movement, shown as mechanosensory and proprioceptive signals (waveform), leg–substrate contact and load (arrows on a surface), odor cues (plume lines), and vision (eye). These signals close the sensorimotor loop and allow simulated behavior to be compared with that of the animal.

2. Digital *Drosophila*: Resources and Data Products

2.1. Anatomical Coverage Is Part of the Model Specification

Each connectomic resource is defined by a specimen, a sampled region, an imaging modality, a voxel size, a reconstruction protocol, and a set of inclusion rules, and together these choices determine which questions it can answer [20,21]. A whole-brain dataset is well suited to global network statistics and long-range pathways [7,22], but without the VNC it cannot show how descending commands reach the leg and wing motor neurons [15,23,24]. A brain-and-VNC volume improves anatomical continuity, although coverage and proof-

reading status may vary across regions [11]. A partial central-brain dataset such as the hemibrain supports detailed analysis of the circuits it contains, including the central complex and the mushroom body [25–27].

Table 1 maps representative resources onto the roles they can play in an embodied-control study. These resources were acquired with two families of volume EM [28,29]. Serial-section transmission electron microscopy (ssTEM) images successive ultrathin sections with a transmission electron microscope and aligns the images computationally into a volume [9,30,31]. Focused ion beam scanning electron microscopy (FIB-SEM) removes a thin layer of material with a focused ion beam and images the newly exposed block face with a scanning electron microscope, which yields nearly isotropic three-dimensional sampling [32,33]. GridTape combines automated collection of serial sections on tape with automated, high-throughput transmission imaging; it is the acquisition route used for FANC and BANC rather than a separate imaging principle [11,23]. Neuron and synapse counts in the table are those reported in the cited papers; the public datasets continue to be corrected and updated as proofreading proceeds [34]. The table therefore also gives the release identifier where the cited paper or the data provider names one, and the same dataset names are used throughout this review.

Table 1. Representative anatomical resources. EM: electron microscopy; ssTEM: serial-section transmission EM; FIB-SEM: focused ion beam scanning EM; VNC: ventral nerve cord. FAFB and FlyWire are successive imaging and reconstruction layers of the same specimen. Counts are those reported in the cited papers. Release: the identifier of the static release analyzed in, or distributed with, the cited paper; "versioned" indicates an online dataset that is updated in numbered releases, so the release queried should be reported; CAVE: Connectome Annotation Versioning Engine. † Reviewed preprint.

Dataset	Coverage	Acquisition/Scale	Release	Main Use and Limitation
FAFB/FlyWire	Adult female brain; shared specimen	ssTEM; 4 × 4 × 40 nm; 139,255 neurons in FlyWire	FlyWire v783	Brain-wide pathways and network statistics; VNC not included [7,9].
BANC	Adult female brain, neck connective, and VNC	GridTape ssTEM; 4 × 4 × 45 nm	v888 (static snapshot)	Continuous brain–VNC pathways; lamina and ocellar ganglia not reconstructed [11].
hemibrain	Part of the adult female central brain	FIB-SEM; 8 nm isotropic; about 25,000 neurons	v1.2.1 (neuPrint)	Detailed central-brain circuits, including the central complex and mushroom body [25].
MANC †	Male Adult Nerve Cord (VNC) and neck connective	FIB-SEM; 8 nm isotropic; about 23,000 neurons	neuPrint, versioned	Premotor and motor circuits of the VNC; brain not included [15,35].
FANC	Female Adult Nerve Cord (VNC)	GridTape ssTEM; about 4.3 × 4.3 × 45 nm	CAVE, versioned	Leg and wing motor circuits in a female; specimen distinct from BANC [23,24].
Male optic lobe	Right optic lobe of a male	FIB-SEM; 8 nm; about 53,000 neurons, 732 types	v1.0 (neuPrint)	Complete cell-type inventory of one optic lobe [36].
Larval brain	Brain of a first-instar larva	ssTEM; 3016 neurons and about 548,000 synapses	As published	Whole brain at an earlier developmental stage; VNC not included [37].

Whole-brain reconstruction of adult *Drosophila* is now established, and BANC extends serial-section reconstruction along much of the brain–VNC axis of a single animal [7,11]. Peripheral sensory and motor connections, as well as a calibrated dynamical controller, still lie beyond these datasets. Brain-only and VNC-only resources therefore remain comple-

mentary, and combining them across specimens relies on cell-type correspondence, which comparative connectomics has made increasingly practical [38,39].

2.2. From Wiring Diagram to Circuit Function

At the most concrete level, a connectome supplies nodes, edges, spatial locations, cell types, and, in most public datasets, synapse counts with confidence scores [7,40]. These objects support analyses of motifs, recurrent loops, convergence, divergence, path length, and modularity [22,41]. Such structure has repeatedly guided functional hypotheses: the wiring of the medulla suggested a candidate circuit for visual motion detection [42], and the central-complex connectome revealed motifs suited to vector computation [26]. A wiring diagram does not, however, define a unique dynamical system [13,43]. An edge records an anatomical synapse rather than a calibrated synaptic conductance. Synapse counts indicate potential strength but do not resolve release probability, receptor composition, or short-term plasticity [44]. The sign of a connection depends on the receptor as well as on the transmitter; in the *Drosophila* olfactory system, for example, glutamate acts as an inhibitory transmitter [45]. Current *Drosophila* connectomes annotate chemical synapses [7,25], so electrical coupling through gap junctions is largely absent from the graph, and neuromodulators can reconfigure a fixed anatomical circuit into functionally distinct networks [13,14]. In a model of two competing rhythmic oscillators linked to a hub neuron, several different changes in electrical and inhibitory synaptic strength were each sufficient to switch the hub from one rhythm to the other, with the wiring unchanged [46].

This gap matters for control. When a graph is used as a fixed policy, its outputs are determined by the chosen neuron model, weight rule, input encoding, output readout, and body interface [12]. A model can therefore be connectome-constrained and still embody substantial engineering choices. Pospisil et al. make this explicit by combining the connectome, used as a prior, with stochastic optogenetic perturbations to estimate the causal interactions between neurons, which they call the effectome [47]. A modeling study should accordingly report which properties are fixed by anatomy, which are estimated from physiology, and which are learned for the target task.

These distinctions can be organized into four levels of evidence.

1. Anatomical evidence: which cells and synaptic contacts exist in the reconstructed volume.
2. Circuit evidence: which pathways and motifs are supported by connectivity, cell type, location, and comparative data.
3. Dynamical hypothesis: how membrane states, synapses, neuromodulators, and delays transform inputs into outputs.
4. Embodied-control claim: whether the resulting controller improves a physical task under a specified body, environment, and perturbation protocol.

Each level adds assumptions to the one below it, and the same anatomical graph can support several models with different control properties [48,49]. Keeping the levels separate makes it clear which conclusions follow from the reconstruction and which follow from modeling choices.

Within these levels, we also label the status of each claim. [V] marks a finding tested experimentally in *Drosophila*, for example by physiology, optogenetic perturbation, or behavior. [C] marks a computational prediction or simulation result that has not been tested in the animal, or has been tested only in part. [P] marks a proposed engineering application or design principle. The labels are used in Tables 4, 7 and 9, and in the text where the distinction matters. They are not interchangeable. A controller that reproduces a behavior in simulation provides [C] evidence that the chosen graph, dynamics, and body are sufficient for the task under the modeler's assumptions, but it is not [V] evidence that *Drosophila*

produces the behavior in the same way. Successful simulated behavior therefore does not by itself demonstrate biological accuracy.

Figure 2 arranges representative milestones on three parallel tracks. The anatomical track (blue) begins with the FAFB EM volume of 2018, which provided whole-brain images together with targeted reconstructions [9]. The hemibrain added a densely proofread connectome of much of the central brain in 2020 [25]; the first-instar larval brain followed as the first complete connectome of an insect brain [37]; FlyWire completed the adult brain from the FAFB images [7]; and BANC joined the brain to the VNC in a single animal [11]. The executable-model track (teal) starts with FlyBrainLab, which links circuit exploration to executable models [50], and reaches, in 2024, a task-trained connectome-constrained model of the visual system [51] and a spiking model of the entire adult brain [52]. The embodied-simulation track (orange) proceeds from the NeuroMechFly body model [53] to NeuroMechFly v2 with sensory feedback [17], to FlyBody for whole-body walking and flight [54], and to FlyGM, a preprint that uses the whole-brain graph as a locomotion policy [16]. The rising bands indicate, schematically, the growth of coverage and integration within each track. The tracks increasingly draw on one another: the whole-brain spiking model runs on FlyWire connectivity, NeuroMechFly v2 incorporates a connectome-constrained visual network, and FlyGM couples the FlyWire graph to a simulated body. This convergence of anatomy, dynamics, and embodiment is the subject of the following sections.

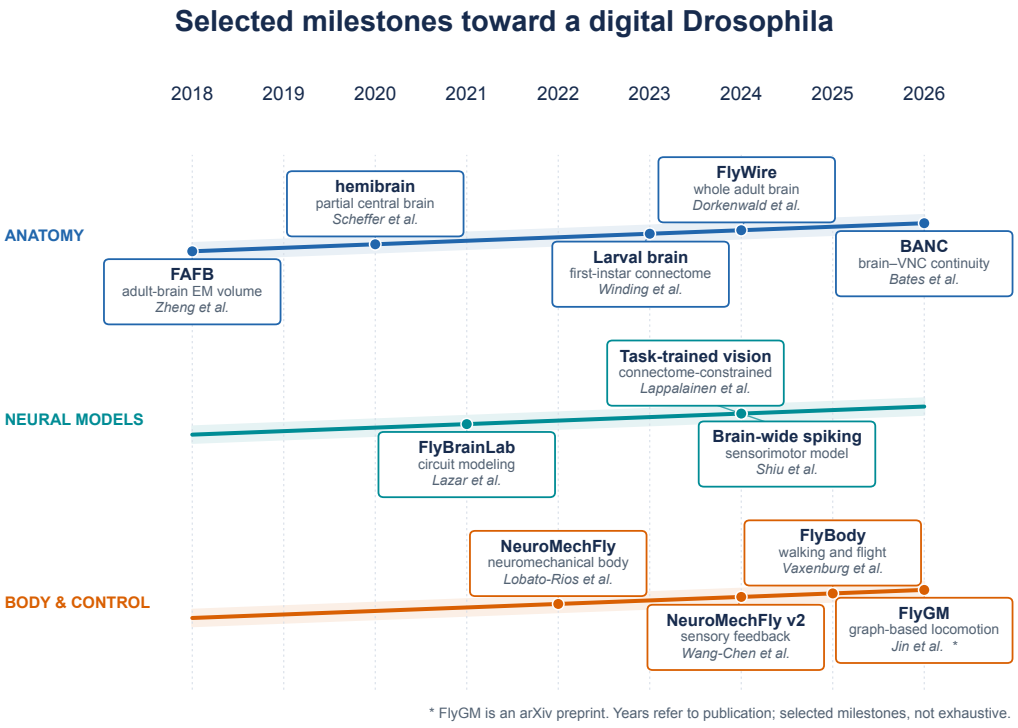


Figure 2. Selected milestones toward a digital *Drosophila*, arranged on three parallel tracks. Blue, anatomical resources: the FAFB adult-brain EM volume [9], the hemibrain partial central-brain connectome [25], the larval-brain connectome [37], the FlyWire whole-adult-brain connectome [7], and the BANC brain–VNC connectome [11]. Teal, executable neural models: FlyBrainLab [50], task-trained connectome-constrained vision [51], and the whole-brain spiking model [52]. Orange, embodied simulation and control: NeuroMechFly [53], NeuroMechFly v2 [17], FlyBody [54], and FlyGM [16], whose asterisk marks an arXiv preprint. Each marker is placed at the year of the cited publication, and the rising bands schematically indicate increasing coverage and integration within each track.

2.3. Dataset Limitations That Matter for Whole-Body Control

For a whole-body controller, the gaps in current datasets matter more than their size. Five classes of limitation are especially relevant.

1. Incomplete sensory periphery.Connectomes reconstruct the central projections of sensory neurons but not the receptor organs that set their tuning, and coverage of the periphery is uneven. In BANC, the lamina and ocellar ganglia are not reconstructed [11], and in the VNC datasets many leg and wing sensory afferents are identified by their nerve of entry and central morphology rather than by the sense organ they come from [15,23,24]. A controller built on these graphs therefore needs a sensory encoder whose properties come from physiology or are chosen by the modeler [18,19].
2. Incomplete motor output. Motor neurons are reconstructed in the VNC datasets and many have been assigned to their target muscles [23,24,35], but neuromuscular junctions, muscle properties, and the mechanics of the exoskeleton lie outside the EM volume. The mapping from motor-neuron activity to force must be supplied by a body model [53,54] and remains a major source of modeling freedom.
3. Uncertain synaptic properties.Edge weights are synapse counts rather than conductances, synaptic signs are inferred from predicted transmitter identity [55], and receptor types, release probability, delays, and short-term dynamics are unmeasured for most connections [44].
4. Missing interaction types. Gap junctions are not annotated, although electrical synapses built from innexins, especially ShakB, are widespread in the *Drosophila* nervous system and are required for normal visual-motion processing and for the intrinsic stability of some visual projection neurons [56]. Neuromodulatory and peptidergic signaling, which can act beyond synaptic contacts, is also absent from a synaptic graph [13,14].
5. Differences between specimens. The adult resources come from different individuals of both sexes and were reconstructed with different pipelines (Table 1). Joint analysis of FlyWire and the hemibrain revealed broad stereotypy, but also occasional variability in neuron counts and connectivity, and about one-third of the cell types proposed for the hemibrain could not be reliably reidentified in FlyWire [38]. A controller derived from one specimen therefore inherits that animal's idiosyncrasies unless its edges are checked across hemispheres and specimens (Section 3.4).

These limitations affect the levels of evidence differently. They leave anatomical evidence about strong, reproducible connections largely intact, but they keep claims at the dynamical and embodied-control levels in the domain of hypothesis, particularly for controllers that span sensing, central processing, and actuation.

3. From Tissue to a Usable Connectome

3.1. Imaging Modalities and the Errors They Introduce

The experimental chain begins with fixation and heavy-metal staining, followed by dehydration, resin embedding, sectioning or surface milling, electron imaging, volume registration, segmentation, synapse annotation, and proofreading [28,57]. As introduced in Section 2, ssTEM gains in-plane resolution and throughput at the cost of axial resolution, whereas FIB-SEM gains isotropic voxels at the cost of throughput; array tomography, which collects serial sections on a solid substrate, additionally allows molecular labels to be combined with ultrastructure [58]. The approaches also differ in section-handling artifacts [29,59].

Each acquisition method leaves characteristic uncertainty in the graph. Section folds, missing sections, anisotropic resolution, charging artifacts, staining variation, and alignment errors can break thin neurites or create false continuities [60,61]. FIB-SEM avoids section

handling but requires drift correction during long acquisitions [33]. In the ssTEM datasets of Table 1, the section thickness of 40–45 nm is about ten times the in-plane pixel size, so a neurite that is clear within one section may be ambiguous across several. Such errors propagate directly into connectivity: a missed branch removes downstream edges, whereas a false merge can create a spurious hub [20]. Elastic registration and large-volume stitching address distinct alignment problems before objects are reconstructed [60,62].

Throughput and sample preparation impose further trade-offs. Automated tape-collecting ultramicrotomy (ATUM), serial block-face scanning EM, thick partitioning for FIB-SEM, multibeam scanning EM, and parallel transmission-EM pipelines raise acquisition throughput in different ways [59,63–66], whereas whole-brain and large-volume en-bloc staining protocols, including one developed for *Drosophila* brains, address the uniformity of contrast [67–69]. For whole-brain projects, the human effort needed for proofreading has become at least as limiting as image acquisition [10,21], and computational correction of axial distortion and section-order errors [61] cannot recover ultrastructure lost during preparation.

A connectome is therefore best treated as an estimate that keeps improving rather than as a fixed measurement. It is assembled from many automated predictions and human corrections, and the public datasets are revised and reissued as numbered versions whenever errors are found [34]. Each step, from the image volume and its alignment through segmentation, synapse prediction, proofreading, and cell-type annotation to the exported graph, should be recorded, so that every neuron and connection can be traced back to the data and edits that produced it. Web interfaces and programming access to the public resources now make this tracing possible [7,34,70]. For a biomimetic model, the same record offers a natural route to uncertainty analysis: alternative edges or cell identities can be sampled according to the confidence scores published with the data [40], and the analysis can then test whether a control conclusion survives.

3.2. Segmentation, Synapse Detection, and Partner Assignment

Neuron segmentation assigns voxels or image fragments to individual neuronal arbors, including branches separated by changes in contrast or by section boundaries [71,72]; it is a separate step from cell typing. Nucleus segmentation locates cell bodies and supports cell counting and registration but does not reconstruct axons or dendrites. Organelle segmentation, for example, of mitochondria, adds subcellular context without measuring energetic state or defining connectivity [73].

Synapse detection identifies candidate presynaptic and postsynaptic specializations in the ultrastructure. Partner assignment then determines which reconstructed neurites lie on the presynaptic and postsynaptic sides of each synapse, including the multiple postsynaptic partners of the polyadic synapses that are common in insects [40]. This second step turns a local synaptic object into a directed graph edge: a detected synaptic density reveals who communicates with whom only once it is linked to two neuron identities. Partner assignment remains uncertain where neurites are fragmented, densely packed, or separated by a poorly resolved cleft.

The remaining tasks include cell-type annotation, registration to a common atlas, proofreading, confidence estimation, and the publication of updated datasets. Automated segmentation makes large volumes tractable, but targeted human review is still required [10,20]. Affinity networks, three-dimensional U-Nets, flood-filling networks, and dense voxel embeddings [71,72,74,75], refined by structured losses and local shape descriptors [76,77], all produce candidate neuronal instances; synaptic partner prediction then links detected synapses to them [40], and a record of every proofreading edit makes each part of the

exported graph traceable to its source [10,34]. Table 2 lists these data products separately because their errors affect a controller in different ways.

The evaluation metric must match the data product. Benchmarks show that boundary-overlap scores can diverge from measures of object identity or topological continuity [78–80]. A topology-preserving loss for tubular structures, for instance, rewards continuous neurites but does not test whether the correct presynaptic and postsynaptic neurons have been paired. For a connectome used as a control prior, geometric overlap, neurite continuity, neuron identity, synapse detection, and partner assignment are best reported as separate quality dimensions.

Table 2. From image data to graph objects. The definitions separate anatomical measurements from the relations that a model infers from them.

Data Product	Operational Definition	What It Contributes, and What Can Go Wrong
Registration	Alignment of sections or block-face images into a common coordinate system	Makes neurite tracing and atlas mapping possible; local warps or missing sections can change apparent branch continuity.
Neuron segmentation	Assignment of image voxels or fragments to one neuronal arbor	Produces graph nodes and neurite geometry; false splits delete paths, while false merges create artificial hubs.
Cell-nucleus segmentation	Detection of nuclear regions and cell-body landmarks	Supports counting, localization, and atlas registration; a nucleus is not a complete neuronal reconstruction.
Mitochondrial segmentation	Detection of mitochondria within neurites or cell bodies	Adds subcellular context for metabolic or synaptic hypotheses; it does not by itself define connectivity.
Synapse detection	Identification of candidate synaptic specializations in the ultrastructure	Produces candidate local communication events; false positives and missed small synapses alter edge density.
Partner assignment	Linking each synaptic event to the reconstructed presynaptic and postsynaptic neurite identities	Converts a synaptic object into a directed edge; ambiguous neurite continuity or polarity can misassign the communicating pair.
Cell-type annotation	Assignment of a neuron to a type or class using morphology, connectivity, location, and molecular evidence	Enables module-level comparisons; type labels may be probabilistic, may change between dataset versions, or may be incomplete.
Proofreading and dataset updates	Human or algorithmic correction, with each updated dataset published under its own version number	Makes the graph checkable; successive versions can change counts and inferred motifs, so model results should name the dataset version used.

The graph becomes more useful when its annotation and access layers are treated as part of the data product. Proofreading prioritization (NEURD), morphological search (NBLAST), and multi-connectome cell typing relate morphology and connectivity to cell types [38,81,82]; CATMAID, neuPrint, webKnossos, NeuTu, guided-proofreading interfaces, BossDB, and the natverse toolbox provide annotation, query, editing, and analysis access [70,83–89]; and common brain and VNC templates support spatial comparison across specimens [90]. Because each tool exposes a different stage of the pipeline, the result of a graph query depends on which version of the dataset was queried.

3.3. A Layered Graph for Model Builders

For an embodied-control study, the most useful representation is often not the raw EM volume but a layered graph with explicit metadata. A minimal node record includes an identifier, anatomical compartment, cell-type label with its confidence, and the dataset version it comes from; a minimal edge record includes direction, synapse count or confidence, anatomical location, and whether the relation is direct, inferred, or aggregated. Public datasets already provide most of these fields [7,38,70]. When a model uses a population or cell-type graph, the aggregation rule should be recorded, because averaging can hide reciprocal motifs and rare but behaviorally important pathways [22,41].

The next layer adds dynamics. Edges can be converted into signed or unsigned weights, delays, and synaptic filters, with signs informed by predicted neurotransmitter identity [55]. Nodes can be assigned leaky integrate-and-fire, adaptive spiking, graded-rate, or conductance-based dynamics [51,52,91,92]. The final layer specifies the sensory and motor interfaces; without them, a graph model is a neural network in isolation rather than an embodied controller. This layered view lets a reviewer or engineer ask, at every stage, whether a reported effect arises from anatomical topology, from the chosen dynamics, from training, or from the body through which the controller acts.

3.4. Reproducible Use of Heterogeneous Connectome Datasets

Embodied-control studies increasingly combine resources, for example a brain graph from FlyWire with a VNC graph from MANC or FANC or a hemibrain circuit with FlyWire neurons of the same type. Because these datasets differ in specimen, sex, imaging, segmentation, synapse detection, and release (Table 1), a combined graph is itself a modeling product. We recommend six practices.

1. Pin and report versions. Record the dataset name, the release or materialization identifier (for example, FlyWire v783, hemibrain v1.2.1, or BANC v888), the versions of the annotation tables, the date of each query, and the query code, and archive the exported graph with a checksum [34,70]. Live databases continue to change, so a model that names only the resource cannot be reproduced.
2. Match across specimens explicitly. Map neurons between datasets at the level of cell types, combining morphology, compared by NBLAST after bridging registration to common templates, with connectivity [38,82,90]. Report the matching rule, its confidence, and the fraction of neurons or synapses that could not be matched, and avoid one-to-one neuron correspondences that the data do not support.
3. Define edge inclusion. State the synapse-confidence cutoff, the minimum synapse count required to accept an edge, and how polyadic synapses and autapses were handled [7,40].
4. Test sensitivity to uncertain edges. Repeat the main analysis while sweeping the synapse-count threshold, resampling edges according to their confidence scores [40], and removing or reweighting connections that are not reproduced across hemispheres or specimens [38]. Report a control conclusion together with the range of graphs over which it holds.
5. Document the seams between datasets. Where a brain graph and a VNC graph from different animals are joined through descending and ascending neuron types [35,39], report the joining rule, and test whether the conclusions change when the seam is perturbed or when the single-animal BANC graph is used instead [11].
6. Release derived artifacts. Publish the derived graph, the cell-type matching tables, the rules used to convert synapse counts into weights, and the model code, so that the study can be rerun on a later release.

4. Connectomes as Structural Priors for Executable Models

4.1. Three Levels of Biological Constraint

Using a connectome can entail quite different modeling commitments, and we distinguish three levels. At the first level, a study extracts a computational principle and implements it in a new architecture without preserving anatomical identity. Examples include a similarity-search algorithm derived from the expansion and sparsification of *Drosophila* olfactory coding [93], a continual-learning architecture modeled on the mushroom body [94], and compact recurrent controllers inspired by the nematode nervous system [95]. At the second level, a reconstructed module is embedded into an artificial controller, preserving selected neuron classes and connections while adapting their interfaces; the connectome-constrained visual network that NeuroMechFly v2 uses for visually guided fly following is an example [17,51]. At the third level, a large connectome supplies the controller topology and only a limited set of parameters is learned or calibrated, as in whole-brain graph policies for simulated locomotion [16]. No level is universally preferable. The first is often the most transferable, the second preserves a recognizable circuit mechanism, and the third provides the strongest structural test but is the most sensitive to missing biology.

This distinction avoids an unhelpful binary between biological and non-biological models. A model can be biologically motivated because it inherits a routing or dynamical constraint even if its neurons are not one-to-one copies. Conversely, a large graph can be faithful at the level of edges while remaining weakly grounded at the level of dynamics and embodiment.

4.2. From Anatomical Edges to Trainable Dynamics

A graph constrains communication but leaves the update rule open [12]. Let A_{ij} indicate whether neuron j connects to neuron i in a selected reconstruction, and let W_{ij} denote a trainable interaction strength. A hard topological prior can then be written as

$$h_{t+1} = f_\theta\big(h_t, (A \odot W)h_t, E_\phi(o_t)\big), \qquad a_t = D_\psi(h_t), \tag{1}$$

where h_t is the neural state, o_t is the observation, a_t is the action, E_ϕ is a sensory encoder, D_ψ is a motor decoder, and $\odot$ denotes elementwise multiplication. Equation (1) expresses in generic form the structure shared by the models discussed in this section, and it makes the division of responsibility explicit: anatomy restricts which interactions are possible, whereas the dynamics f_θ, the encoder, and the decoder must still be specified. A soft prior instead permits additional edges but penalizes departures from the anatomical graph, for example, by adding a sparsity penalty on non-anatomical weights to the task loss,

$$\mathcal{L} = \mathcal{L}_{\text{task}} + \lambda \|(\mathbf{1} - A) \odot W\|_1, \tag{2}$$

where $\mathbf{1}$ is the all-ones matrix and λ sets the strength of the anatomical prior. Cell-type parameter sharing adds a further constraint by assigning common parameters to neurons or connections of the same type [51].

Shiu et al. built a leaky integrate-and-fire model of the entire adult brain from FlyWire connectivity and predicted neurotransmitter identity [52]. Each model neuron integrates its input, leaks toward rest, and emits a spike at threshold. Activating sugar- or water-sensing gustatory neurons in the model identified neurons required for feeding initiation, and activating mechanosensory neurons recruited a small antennal-grooming circuit; selected predictions were then confirmed in *Drosophila* by optogenetic activation and behavioral experiments. For engineering, the main contribution is an anatomically indexed system for signal propagation and intervention, which can serve as a starting point for a closed-

loop locomotion policy. The transmitter predictions that set synaptic signs are themselves inferred from EM images rather than measured at every synapse [55].

Lappalainen et al. followed a different route [51]. They built a model of 64 cell types in the motion pathways of the *Drosophila* optic lobe with experimentally determined connectivity, and then optimized the unknown single-neuron and synaptic parameters so that the network estimated optic flow, the apparent motion of a visual scene, from naturalistic video. Neural recordings were not used for training; instead, the model's predictions were compared with measurements from 26 previously published studies. The study therefore shows how anatomy and a computational task can jointly constrain functional predictions, and it reports that this strategy works best when the underlying connectivity is sparse. Because several parameter settings can solve the task comparably well, the authors analyzed an ensemble of independently trained models rather than a single solution.

Together, these studies separate broad anatomical coverage from task-specific parameter identification. Shiu's model is spiking, whereas Lappalainen's uses graded, non-spiking units, so the two do not settle whether spiking dynamics confer an advantage for control. Rate networks and recurrent policies remain useful comparators, especially when the question is whether topology or neuron complexity explains performance, and surrogate-gradient methods now allow spiking and rate networks to be trained with the same optimizers [96]. Biologically constrained recurrent networks can also impose excitatory and inhibitory organization without measured *Drosophila* connectivity [97]. Sign constraints, sparsity, cell-type sharing, and individual anatomical edges should therefore be tested as separate contributions.

Task performance also does not identify a unique mechanism. Distinct circuit parameters can generate similar network activity [48,49], and systems-biology models often contain parameter combinations that are poorly constrained by the available observations [98]. A connectome-constrained controller may therefore be useful while several dynamical explanations remain open. Pathway ablations, activity predictions, and comparisons with simpler recurrent or rate-based models are needed before a fitted controller is interpreted as a reconstruction of biological computation.

These ambiguities limit the biological interpretation of a successful connectome-constrained controller in two ways. The first is parameter non-identifiability. When many combinations of time constants, gains, and synaptic scales give the same task performance, a single fitted value carries little biological meaning. What can be interpreted is a property shared across the ensemble of good solutions, as in the ensemble analysis of Lappalainen et al. [51], or a prediction that holds whichever solution is chosen [48,98]. The second is omitted mechanisms. A model without gap junctions or neuromodulation can compensate for their absence by adjusting the parameters it does have. Electrical synapses are widespread in the *Drosophila* nervous system and contribute to motion processing and neuronal stability [56], and neuromodulators can switch the output of a fixed circuit [14,46]. A chemical-synapse model fitted to the same behavior may therefore assign the work of these mechanisms to chemical weights or to the decoder. In either case, a successful controller shows that the reconstructed topology is sufficient for the task under the chosen assumptions. It shows neither that *Drosophila* uses the same mechanism nor that the individual parameter values are physiological. Table 3 separates parameters with physiological support from those that are inferred or set for engineering reasons so that a study can state which of its conclusions rest on each kind.

Table 3. Parameter provenance in connectome-constrained models. Support: *measured*, determined by anatomical or physiological measurement; *inferred*, predicted from indirect data; *engineering*, set or fitted by the modeler for the task; *omitted*, absent from current models.

Model Quantity	Typical Source in Current Models	Support	Consequence for Interpretation
Existence and direction of connections	EM reconstruction and synaptic partner assignment [7,40]	Measured, with proofreading error	Strongest constraint; conclusions should be checked against uncertain edges.
Connection strength	Synapse count scaled by a global factor [52] or by fitted cell-type-pair factors [51]	Count measured; scale engineering	Relative strengths are anatomical proxies; absolute gains are not physiological.
Synaptic sign	Transmitter identity predicted from EM images and mapped to excitation or inhibition [55]	Inferred	Receptor-dependent exceptions, such as inhibitory glutamate [45], can reverse predicted effects.
Time constants, thresholds, and refractory periods	Shared values for all neurons [52] or task optimization [51]	Engineering; measured only for selected cell types	Often non-identifiable; interpret only properties that are robust across an ensemble.
Cell-type parameter sharing	Assumption that neurons of one type share parameters [51]	Supported anatomically by type-level stereotypy [38]	Reduces free parameters but can hide variability within a type.
Synaptic delays and short-term dynamics	Fixed constants or omitted	Largely unmeasured [44]	Conclusions that depend on timing remain hypotheses.
Sensory encoder and motor decoder	Hand-designed filters or learned networks [16,17]	Engineering	May carry much of the task performance; must be ablated or matched across baselines.
Gap junctions	Not annotated in current connectomes	Omitted; electrical synapses are widespread in *Drosophila* [56]	Their function may be absorbed by other parameters.
Neuromodulation and behavioral state	Omitted, or represented as a global gain	Omitted; compartment-specific modulation is measured [99,100]	State-dependent behavior lies outside the model's claims.

4.3. Navigation, Association, and Distributed Motor Organization

The central complex, a group of interconnected neuropils involved in navigation and action selection, offers a concrete example of principle-level transfer. Functional studies show a persistent heading representation anchored to visual landmarks [101], ring-attractor dynamics [102], and updating of the heading estimate by angular velocity during turns [103,104]. A ring attractor is a recurrent network that maintains a localized bump of activity whose position encodes a circular variable such as heading [105]. The central-complex connectome identifies recurrent and columnar motifs that could implement these computations and transform compass signals into a navigation state [26]. Its engineering counterpart is therefore best assessed as a state estimator under cue loss or cue conflict, with explicit tests of state maintenance, sensory anchoring, and movement-dependent updating, rather than as a generic recurrent network with a ring-shaped diagram.

The distinction between heading and travel direction adds an interface requirement, because a fly or a robot may move sideways while facing forward. Lyu et al. showed how an allocentric travel-direction signal is built by vector computation, and Lu et al. traced how movement signals are transformed from body-centered to world-centered coordinates [106,107]. These results motivate explicit coordinate transformations between perception, internal state, and motor commands. Turning a travel vector into a home vector requires a further integration stage, such as the anatomically constrained path-integration circuit proposed for the bee central complex [108].

Visual motion shows why the sensory front end cannot be treated as a neutral input layer. Directional tuning emerges through successive stages of the *Drosophila* motion pathway, and connectomic analyses of the ON-motion circuit identify the synaptic organization available for that computation [42,109–111]. The temporal tuning of motion detectors is further shaped by the dynamics of their input neurons [112]. A transferred visual module

should therefore report its receptive-field geometry, temporal filtering, and learned encoder rather than attributing all optic-flow behavior to downstream graph topology.

Mushroom-body circuits solve a different problem: learning associations between sensory representations and their behavioral significance. Complete connectomes of the larval and adult mushroom bodies show an expansion from olfactory projection neurons onto many Kenyon cells, followed by convergence onto a small set of output neurons arranged in discrete compartments [27,113]. Sparse, decorrelated odor representations in Kenyon cells improve the learned discrimination of similar odors [114], and compartment-specific dopaminergic inputs provide a basis for selectively modifying associations [100,115]. Output neurons, by contrast, show broader and correlated odor tuning that differs between individuals as a result of plasticity [116], and compartmentalized neuromodulation changes processing with state and experience [99]. Bennett et al. formalized reinforcement-prediction-error learning in a mushroom-body model [117]. For an artificial controller, these studies suggest separating a stable sensory expansion, an adaptable readout, and a modulatory signal rather than treating all connections as equally plastic, an arrangement that has already been shown to reduce catastrophic forgetting in continual learning [94].

Motor organization also departs from a simple top-down hierarchy. Descending networks transform command signals into distributed population activity [118], and comparative connectomics maps both descending and ascending pathways between the brain and the VNC [39]. BANC extends this view to interactions between behavior-related modules across the brain and VNC [11]. An engineering hierarchy inspired by these findings should therefore permit local feedback and lateral interactions between modules instead of a strict one-way command tree, consistent with hierarchical motor-control architectures developed for both animals and machines [119].

Behavioral and physiological studies constrain the receiving side of that hierarchy. Descending pathways have been linked to walking direction, behavioral state, and action-specific motor organization [120–122]. In the legs, proprioceptive signals are encoded in separate feature channels and transformed centrally rather than passed on as a copy of joint angles [18,19,123], and motor neurons are recruited in an order related to the force they produce [124]. Connectomic analyses of MANC further resolve how descending inputs reach premotor and motor populations [35]. A controller that maps a brain-level command directly to robot torque therefore makes a substantial interface assumption, and it should be compared with architectures that retain an intermediate motor network or a learned body-specific decoder.

Circuit-level models are also computationally valuable. A model can preserve cell-type and pathway identities while using reduced dynamics, which makes it possible to test interventions without reconstructing every membrane process. Whole-brain network statistics and multi-connectome annotations add constraints on sparsity, heterogeneity, and repeated cell classes [22,38]. These analyses motivate structured policies; whether such policies learn faster or control a body more reliably than dense alternatives is a question for direct comparison.

Platforms such as FlyBrainLab support this work by linking circuit inspection to executable models [50], so that a circuit hypothesis and its computation remain explicitly connected. Table 4 compares representative studies by their anatomical constraints, how the model parameters are obtained, how the models were validated, what they found, and what limits their interpretation.

Table 4. Representative executable models and body platforms. Neural prediction, physical control, and anatomical fidelity are distinct outcomes. Evidence labels (Section 2.2): [V], tested experimentally in *Drosophila*; [C], computational prediction or simulation result; [P], proposed application. † Preprint, not peer reviewed. LIF: leaky integrate-and-fire; RL: reinforcement learning; MLP: multilayer perceptron.

Study/Platform	Anatomical Constraint and Parameter Source	Validation Method	Major Findings (Evidence)	Limitations
Whole-brain spiking model [52]	FlyWire brain connectivity; synapse counts with one global scale; signs from predicted transmitters; shared LIF parameters	Optogenetic activation and behavioral experiments for selected model predictions	Neurons for feeding initiation and an antennal-grooming circuit predicted [C], and selected predictions confirmed in *Drosophila* [V]	Uniform neuron parameters; no gap junctions, neuromodulation, or body feedback; only a few pathways tested
Task-trained visual network [51]	Optic-lobe connectivity of 64 cell types; cell-type parameter sharing; unknown parameters optimized for optic-flow estimation	Predicted neural responses compared with recordings from 26 earlier experimental studies, which were not used to train the model; ensemble of models	Tuning properties of many visual cell types predicted from connectivity and task [C], consistent with existing recordings [V]	One sensory subsystem; graded non-spiking units; several parameter settings solve the task; accuracy depends on sparse connectivity
Central-complex studies [26,101,102]	hemibrain connectivity of the central complex combined with functional imaging and ring-attractor models	Calcium imaging during behavior and optogenetic perturbation	Heading bump with ring-attractor dynamics [V]; connectome-derived circuits for vector computation [C]	Many connectome-derived mechanisms not yet tested; route memory and full navigation open; rarely coupled to a body
Mushroom-body model [117]	Circuit organization (Kenyon-cell expansion, compartments, dopaminergic feedback) rather than synapse-level weights; plasticity rules	Reproduction of published conditioning and blocking experiments	Reinforcement-prediction-error learning implemented by the circuit, with five experimentally testable predictions [C]	Plasticity rules partly hypothetical; not coupled to a body; no whole-connectome weights
NeuroMechFly v2 (FlyGym) [17]	Body morphology and mechanics; sensory interfaces; modular controllers; connectome-constrained visual module for fly following	Closed-loop task performance in simulation	Multimodal closed-loop tasks, including visually guided following [C]	Simplified actuation; controllers designed or trained by the modeler; whole-connectome control not included
FlyBody [54]	Whole-body physics in MuJoCo; no connectome constraint; RL with imitation of recorded *Drosophila* kinematics	Comparison of simulated walking and flight with recorded behavior	Realistic walking and flight [C]	Controllers are artificial networks rather than *Drosophila* circuits
FlyGM † (arXiv, v3) [16]	FlyWire graph as message-passing topology; expert imitation followed by RL in a FlyBody-based fly	Comparison with rewired, random-graph, and MLP policies in simulation	Stable locomotion across tasks and better reported sample efficiency than graph and non-graph baselines [C] †	Not peer reviewed; no neural-activity validation; limited task set; readout and decoder may carry much of the performance

Read together, the studies in Table 4 have complementary strengths and share three limitations. The whole-brain model offers the broadest anatomical coverage and has produced experimentally tested predictions, but its uniform neuron parameters and single synaptic scale mean that its success is chiefly a statement about signal routing rather than about *Drosophila* dynamics [52]. The task-trained visual network makes the most quantitative contact with physiology, yet it covers one well-studied subsystem, was compared with existing recordings rather than new ones, and leaves several parameters undetermined, which its ensemble makes visible rather than resolves [51]. Central-complex and mushroom-body studies have the strongest link between circuit structure and function, because physiology and perturbation data were available before or alongside the connectome; their biological significance is high, but most of the resulting models remain disembodied [26,117]. The body platforms test physical consequences, but, by default,

use controllers that are not *Drosophila* circuits [17,54] and FlyGM, the only whole-graph controller of a whole body, are still preliminary evidence [16]. The shared limitations are that (i) no study yet combines whole-connectome dynamics with a body and validates both against neural recordings; (ii) validation usually compares the model with a few selected measurements rather than testing its full set of predictions; and (iii) simulated task success, where it is reported, is evidence of sufficiency under the modeler's assumptions rather than of biological accuracy. These gaps define the most informative next experiments.

5. Closing the Brain–Body Loop

5.1. A Body Simulator Supplies the Missing Physical Context

An isolated connectome cannot express balance, contact, drag, actuator saturation, or the consequences of moving a particular limb [3,4]. A body simulator supplies these missing variables. In a minimal loop, the controller receives sensory observations, updates its internal state, emits motor commands, and receives new observations after the body interacts with the environment. The body may be a detailed articulated *Drosophila* model, a reduced rigid-body model, a soft robot, or a physical robot with measured dynamics [125], and the biological interpretation of the controller depends on which of these choices are held fixed.

NeuroMechFly established a morphologically and mechanically grounded model of adult *Drosophila* [53]. NeuroMechFly v2, distributed through the FlyGym package, adds vision, olfaction, ascending motor feedback, and complex terrain and demonstrates closed-loop tasks that include fly following with a connectome-constrained visual network [17]. FlyBody instead emphasizes whole-body walking and flight in the MuJoCo physics engine, with neural-network controllers trained by data-driven reinforcement learning [54,126]. The two platforms provide complementary physical contexts, and in both the default controller is designed or trained by the modeler; connectome constraints enter where a study adds them.

Robotics helps separate the contribution of the controller from that of the body. Passive-dynamic walkers generate coordinated gait through mechanics alone [127], and local force feedback can coordinate the legs of a quadruped through physical interaction, without direct neural coupling between the leg oscillators [128]. Although unrelated to *Drosophila* connectomics, these results show that an organized gait can be attributed to neural wiring only when body dynamics and feedback access are held constant.

The contribution of mechanics extends beyond passive walking. Powered bipeds derived from passive-dynamic designs show how body dynamics can reduce the control burden, and theoretical work on compliant bodies shows how mechanical deformation can carry out part of the computation on time-varying inputs [129,130]. MuJoCo provides a general physics engine for articulated bodies with contacts and actuators, whereas NeuroMechFly and FlyBody specify particular animal bodies and control settings [53,54,126]. A physics engine, an animal model, and a trained controller are thus separate artifacts, and each needs its own validation. A salamander robot driven by a spinal-cord model combined rhythmic modules with higher-level gait transitions, an early example of principle-level transfer from a vertebrate locomotor circuit to a machine [131,132].

5.2. Sensory and Motor Interfaces Determine the Meaning of a Graph

The same internal graph can implement different computations when its input and output channels change. A *Drosophila* visual neuron receives temporally filtered signals sampled by a hexagonal lattice of ommatidia [51], whereas a robot camera delivers frames or, in the case of an event camera, asynchronous brightness changes [133]. A descending

neuron acts on a local premotor network, whereas a robot policy may command joint torques directly. Treating these channels as interchangeable hides the main engineering problem.

Insect-inspired robotics makes the interface issue concrete [6,134]. A cricket robot tested a sensorimotor explanation of phonotaxis, AntBot combined a polarized-light compass with odometric cues for outdoor homing, and a bee-inspired hovercraft used optic-flow feedback for corridor guidance [135–137]. A model of ant route navigation based on scene familiarity addresses a different task from path integration [138]. None of these systems uses a *Drosophila* connectome, yet each shows that sensory statistics, temporal filtering, task definition, and the available action variables must be matched before a neural architecture can be credited with a control advantage.

Table 5 lists the interface layers that should be reported and indicates where biomimetic transfer is most promising. Module-level transfer is a tractable compromise: recurrent organization and internal state are retained, while sensor and actuator adapters are redesigned for the receiving body. Whether this preserves the intended computation can be tested directly by comparing adapters that retain or discard the relevant properties of the biological interface.

Table 5. Interface layers required to turn a connectome into an embodied controller. The neural graph is one layer of the closed loop.

Interface	Typical Implementation	Question for Transfer
Sensor → neural input	Receptive-field filters, event streams, learned encoders, or task-defined feature channels	Which properties of the biological sensor are retained, and which are replaced by an adapter?
Within the neural core	Spiking, rate, conductance, or recurrent state dynamics on a fixed or partially learned graph	Is performance due to topology, dynamics, optimization, or their interaction?
Brain → local motor network	Cell-type populations, motor primitives, or a learned decoder	Does the output preserve modular action organization or collapse the graph into a black-box readout?
Neural output → actuation	Joint targets, muscle activations, forces, torques, or low-level policies	How are differences in actuator count, bandwidth, and saturation handled?
Body → ascending feedback	Proprioception, contact, optic flow, inertial state, or task reward	Does feedback close the same computational loop as in the biological hypothesis?
Task learning → parameters	Synaptic plasticity, neuromodulatory gates, policy gradients, or supervised calibration	Which parameters are allowed to adapt, and does adaptation preserve the proposed principle?

The receiving motor system should also be treated as a model component. As discussed in Section 4.3, descending pathways, leg proprioception, and motor-neuron recruitment all shape how a movement command becomes force. A direct map from a graph population to joint torque is therefore an engineering decoder rather than a biological fact. Making that decoder explicit allows a fair comparison between a connectomic high-level module, a controller built from motor primitives [139], and a learned low-level policy [119].

5.3. Large-Scale Graph Policies and Their Attribution Problem

FlyGM directly examines whether a whole-brain connectomic graph can serve as a locomotion controller [16]. Version 3 of this preprint uses the FlyWire graph for message passing in a policy that controls a simulated biomechanical fly built on FlyBody and MuJoCo; the policy is first trained to imitate an expert policy and then refined by reinforcement learning. Comparisons with degree-preserving rewired graphs, size-matched random graphs, and multilayer perceptrons probe whether the measured topology matters. FlyBody thus supplies the body and its learned behavior, whereas FlyGM asks whether a connectome-

derived architecture can replace a generic policy network. The reported tasks provide early engineering evidence for this idea, and *Drosophila* neural dynamics and cross-body generalization are natural next tests.

A whole-brain graph can be used as a policy only after a readout is chosen. One option maps selected descending or motor-related populations to action variables, following the descending-neuron outputs used in whole-brain simulations [39,52]. Another treats the graph as a recurrent latent state and trains a small decoder [16]. A third aggregates cells by type or region, producing a lower-dimensional dynamical system that is easier to optimize [51]. These choices can yield very different controllers from the same connectome.

Low-level control can be supplied by biologically inspired or generic motor systems. A six-legged walking machine combined central pattern generation with local feedback and an adaptive forward model, and reinforcement-learned policies have transferred dynamic locomotion from simulation to physical quadrupeds [140,141]. A comparison should state whether rhythmic coordination, contact correction, and prediction are provided by the body interface or learned by the connectomic graph; otherwise, a strong motor decoder can hide the contribution of the neural topology.

The most informative experiments are therefore causal and matched. One pathway can be removed or randomized while the number of parameters is preserved. Edge identities can be shuffled while in-degree and out-degree are matched [142], as in the rewired graphs of FlyGM [16], or the graph can be replaced by a modular random graph with the same community sizes [143]. Topology can be frozen while the dynamics are retrained, and the dynamics frozen while the readout is retrained. Each variant should then be evaluated under sensor noise, delay, body perturbation, terrain change, and unseen task combinations. This design distinguishes a useful structural prior from an incidental benefit of model capacity or training.

5.4. From Simulated to Physical Bodies

A connectome-constrained controller that works in simulation faces the same reality gap as any learned controller, and possibly a larger one, because its structure was not chosen for the receiving hardware [144]. Five sources of mismatch are especially relevant (Table 6). Actuator delay and limited bandwidth change the phase of feedback; in legged robots, explicit actuator models, or actuator networks learned from measured data, were essential for transfer [141,145]. Contact and friction are among the least accurate aspects of rigid-body simulation, and small errors change slip, ground reaction forces, and gait stability [126]. Sensor noise, bias, and latency differ between a simulated observation and a physical encoder, inertial unit, or camera, and a recurrent controller may integrate such errors into its internal state. Mechanical compliance and unmodeled dynamics alter the body for which the controller was trained. Finally, scale matters. At insect size, flapping flight requires very fast actuation and feedback, and an insect-scale robot depends on actuators and control loops that differ greatly from those of the animal [146]; a larger robot operates under a different scaling of inertia and gravity. A *Drosophila*-derived controller transferred to a robot must therefore be retimed and rescaled, not copied.

Table 6. Simulation-to-reality gaps for connectome-constrained controllers, mitigation strategies, and robustness tests. Each mitigation should be applied equally to the matched baselines.

Gap	Effect on the Controller	Mitigation	Robustness Test
Actuator delay and bandwidth	Shifts the phase of feedback; can destabilize recurrent loops tuned in simulation	Actuator modeling, learned actuator networks, latency randomization [141,145]	Performance as added delay increases
Friction and contact	Changes slip and the load feedback on which the controller relies	Randomized friction and contact parameters; varied training terrain [147,148]	Performance across friction coefficients and terrains
Sensor noise, bias, and latency	Corrupts state estimates; errors can accumulate in recurrent state	Noise and latency randomization; observation dropout during training [149,150]	Estimation error under noise, dropout, and distractors
Unmodeled dynamics and compliance	Mismatch between the trained and the real body	System identification; online adaptation modules [145,151]	Performance with payloads and weakened actuators
Scale and morphology	*Drosophila* time constants and forces do not match the robot	Retiming and rescaling of interface adapters; body–controller co-design [146,152]	Transfer across bodies of different size and morphology

Mitigation strategies from robotics apply directly. System identification and actuator models reduce the gap at its source [141,145]. Domain randomization over masses, friction, motor strength, sensor noise, and latency trains policies that tolerate a range of bodies [147,148], and adaptation modules estimate changing conditions online [151]. For a connectome-constrained controller, these strategies should be applied in the same way to the matched baselines, and transfer should follow a standard robustness protocol: performance under graded increases in delay, sensor noise, friction change, payload, and actuator weakening, reported as degradation curves rather than as single success rates. Such curves would show directly whether recurrent or modular structure taken from the connectome makes a controller degrade more gracefully than a generic network, which is one of the advantages most often claimed for biologically structured controllers (Section 6.2).

6. What Can Transfer to Other Embodied Agents?

6.1. From Anatomy to Engineering Hypotheses

The most portable lessons are organizational rather than anatomical. A region name is tied to a species and a body, whereas a principle such as sparse communication or recurrent state estimation can be tested on many platforms [6,125]. Table 7 summarizes five candidate design principles and one methodological principle. For each, it gives the *Drosophila* evidence that suggests it, labeled by evidence status, states whether the principle was already established in computational neuroscience or robotics, and pairs it with an engineering test that could refute it.

The strength of *Drosophila*-specific support therefore differs across the principles. Recurrent state estimation and selective plasticity rest on the strongest *Drosophila* evidence, because physiology and perturbation experiments have tested the circuit mechanism and the connectome has resolved its wiring [26,100,102]. Sparse modular communication and hierarchical motor control were established in computational neuroscience and robotics before *Drosophila* connectomes existed; the connectome adds quantitative anatomical constraints, but their functional advantages have not been tested in *Drosophila* itself [22,119,153]. Body–controller co-design comes mainly from embodiment research, and *Drosophila* data illustrate rather than establish it [1]. Anatomically indexed intervention is the contribution most specific to connectomics, although it is a method rather than a property of a controller. We therefore count five candidate design principles and one methodological principle.

Table 7. Candidate biomimetic principles, the *Drosophila* evidence that motivates them, their origin, and tests that could confirm or refute them in embodied agents. The first five rows are design principles for controllers; the last row is a methodological principle for analyzing them. Evidence labels as in Section 2.2; every principle is itself a proposal [P].

Candidate Principle	*Drosophila* Evidence (Status)	Origin: Established Elsewhere, or *Drosophila*-Derived	Discriminating Test
Design principles			
Sparse modular communication	Sparse, heterogeneous whole-brain connectivity with repeated cell classes, local circuits, and long-range projections [22,38] [V, anatomical]; functional benefit not tested in *Drosophila*	Established: modularity and sparse, energy-efficient coding in network science and neuroscience [153,154]; *Drosophila* connectomes add synapse-level constraints on module size and routing	Compare generalization and energy use with dense recurrent baselines at matched parameter counts.
Recurrent internal state	Heading bump with ring-attractor dynamics shown by imaging and perturbation [101,102] [V]; recurrent and columnar motifs in the connectome [26] [V, anatomical; mechanism C]	Theory established [105]; *Drosophila* supplies the most direct anatomical and functional confirmation, so this principle is the most strongly *Drosophila*-derived	Add observation dropout, delay, and distractors; measure drift, recovery, and calibration.
Hierarchical motor control	Distributed descending population codes [118] [V]; brain–VNC and descending-to-motor connectivity [11,35] [V, anatomical; control roles C]	Established in motor neuroscience and robotics [119]; *Drosophila* connectomes add identified interfaces and evidence for lateral and ascending interactions rather than a strict command tree	Perturb one limb or actuator; test whether unaffected modules preserve useful behavior.
Selective plasticity	Compartment-specific dopaminergic learning in the mushroom body [100,115] [V]; transferred to continual learning [94] [C]	Related ideas established in machine learning [155]; the specific architecture (a fixed sparse expansion with a compartmentalized, modulated readout) is *Drosophila*-derived	Compare fast adaptation, forgetting, and interference with globally plastic controllers.
Body–controller co-design	Proprioceptive feature channels [19] [V]; neuromechanical models show that body and sensors shape control [17,54] [C]	Mainly established in embodiment and robotics [1,152]; connectome-specific support is limited	Test transfer across morphology and dynamics, not only across random seeds.
Methodological principle			
Anatomically indexed intervention	Model-predicted pathways confirmed by optogenetic activation [52] [V for selected predictions]; connectome-guided estimation of effective connectivity [47] [P]	Specific to connectomics: the graph supplies named sites for module, pathway, and cell-type perturbations	Use causal ablations and replacements to link performance changes to graph structure.

6.2. Comparison with Conventional Controllers

A connectome-constrained controller is worth its cost only if it offers something that established controllers do not. Table 8 compares the main families of controllers on the properties most relevant to that question. Central pattern generators with reflexes encode rhythm and coordination explicitly and work well on hardware, but must be designed by hand for each body and task [131,140,156]. Model-predictive control optimizes actions over a horizon using an explicit dynamics model and achieves robust dynamic locomotion on legged robots but relies on an accurate model and hand-chosen costs [157]. Generic deep reinforcement-learning policies, such as multilayer perceptrons and recurrent networks, have produced the most capable learned locomotion to date and transfer to hardware with randomization and adaptation [141,149–151], but they require large amounts of simulated experience and are difficult to interpret. Compact biologically inspired networks such as neural circuit policies are small and inspectable but do not use measured anatomy [95].

Table 8. Connectome-constrained and conventional controllers compared. Hardware evidence refers to demonstrations on physical robots. CPG: central pattern generator; MPC: model-predictive control; RL: reinforcement learning; MLP: multilayer perceptron; RNN: recurrent neural network. † Preprint, not peer reviewed.

Controller Family	Source of Structure	Data and Design Effort	Interpretability	Hardware Evidence	Status
CPG with reflexes	Hand-designed oscillators and feedback, often bioinspired	Little data; substantial design effort for each body	High: explicit rhythm and phase variables	Extensive [131,156]	Established
MPC	Explicit dynamics model and cost function	Little data; requires an accurate model and tuning	High at the level of the model	Extensive for dynamic quadrupeds [157]	Established
Generic deep RL (MLP or RNN)	Network architecture only	Large amounts of simulated experience; randomization for transfer	Low	Extensive [141,150]	Established
Compact bioinspired network	Design motifs from the nematode nervous system	Moderate	High: few neurons	Lane keeping learned from real driving data [95]	Established for selected tasks
Module-level connectome	Measured wiring of one circuit with learned interfaces	Moderate; interfaces must be engineered	Moderate to high: identified cell types	Simulation only [17]	Proposed [C]
Whole-graph connectome	Whole-brain topology with learned readout	High: large graph, imitation and RL	Moderate: anatomically indexed but large	Simulation only [16]	Preliminary [C] †

Against these baselines, connectome-constrained controllers offer three potential advantages, each a hypothesis rather than an established result [P]. First, the measured topology may act as an inductive bias that improves sample efficiency or generalization at a fixed parameter budget. Second, the graph supplies named, anatomically indexed sites for ablation and intervention, which makes failure analysis more interpretable than in a dense network [47,52]. Third, modular and recurrent structure may yield graceful degradation under sensor loss or actuator damage. Concrete costs stand against these advantages: sensory encoders and motor decoders must be engineered for each body (Section 5), large graphs are expensive to simulate and train, and most anatomical detail concerns the *Drosophila* body rather than the target robot.

The current evidence for these advantages is limited. To our knowledge, no peer-reviewed study has compared a connectome-constrained controller with a central-pattern-generator, model-predictive, or generic learned controller on a physical robot under matched sensing, actuation, and training budgets. In simulation, FlyGM reports better sample efficiency than degree-preserving rewired graphs, random graphs, and multilayer perceptrons [16], and the task-trained visual network shows that connectivity together with a task can predict neural responses, most accurately when the connectivity is sparse [51]. Both results concern simulated systems, and the first is a preprint. Neural circuit policies and Rapid Motor Adaptation, which separates a locomotion policy from an adaptation module [95,151], are useful baselines precisely because they do not use *Drosophila* anatomy. A connectome-constrained controller should receive the same sensing, encoding, motor decoding, parameter budget, and adaptation opportunities as each conventional baseline before any benefit is attributed to measured wiring.

6.3. Testable Predictions

Table 9 turns the principles of Table 7 into specific predictions. Each states a measurable outcome, the matched baseline against which it is measured, and the result that would falsify it. All are proposals [P]; none has yet been tested in the form stated here.

Table 9. Falsifiable predictions for connectome-derived design principles. "Matched" means equal numbers of trainable parameters, identical sensor and actuator interfaces, the same training budget, and multiple random seeds.

Principle	Prediction	Measurement and Matched Baseline	Falsified If
Sparse modular communication	A controller with connectome-derived sparse modular topology [22] retains more performance on held-out terrains and tasks, at lower energy per distance, than a dense recurrent network	Held-out return and cost of transport [129]; dense RNN, degree-preserving rewired graph, and community-matched random graph [142,143]	No advantage beyond seed-to-seed variability, or the same advantage obtained by the community-matched random graph, which would credit modularity rather than measured wiring
Recurrent internal state	A ring-attractor heading module [102,105] maintains its heading estimate during cue loss with slower error growth, and re-anchors faster when cues return, than a gated recurrent estimator of equal size	Heading error over time without cues and recovery time after cue return; gated recurrent network, such as a long short-term memory or gated recurrent unit network [158,159]	Drift and recovery are no better than those of the baseline
Hierarchical motor control	With a separate body-specific motor layer [119], failure of one actuator is compensated with less retraining and with less loss of function in unaffected limbs than in a flat policy	Performance after actuator failure and retraining steps to recovery [160]; flat policy [141]	The flat policy recovers equally fast and fully
Selective plasticity	Restricting plasticity to a modulated, compartmentalized readout [94,100] reduces forgetting during sequential tasks while preserving the speed of learning new tasks	Retention of earlier tasks and new-task learning rate; global fine-tuning and elastic weight consolidation [155]	No reduction in forgetting, or a large loss of learning speed
Body–controller co-design	Interface adapters optimized jointly with body parameters [152] transfer across morphologies better than adapters tuned for one body	Performance after changes in limb length, mass, or actuator count; adapters tuned for a single body, or an online adaptation module [151]	Transfer is no better than with single-body adapters
Anatomically indexed intervention	Ablating a connectome-identified pathway in a trained controller [52] produces a specific, predicted deficit, whereas ablating a random set of equal size produces diffuse deficits	Behavior-specific performance after ablation; size-matched random ablations [161]	Deficits after pathway ablation are indistinguishable from those after random ablation

6.4. Uncertainty, Transfer, and Validation

Transfer can be evaluated at three levels. At the representation level, does a connectome-constrained controller produce useful state variables or features? At the control level, does it improve stability, efficiency, robustness, or learning speed? At the scientific level, does an intervention support the proposed circuit interpretation [134]? A controller can succeed at the first two levels without supporting a biological claim, and a biologically plausible model can fail at the second level because its body interface is poorly chosen.

Uncertainty enters at every level. Anatomical uncertainty can be represented by alternative edge sets, by sampling graphs according to synapse-confidence scores [40], and by comparing homologous circuits across individuals and datasets [38,162]. Dynamical uncertainty can be represented by ensembles over time constants, signs, and delays [48,51]. Embodiment uncertainty can be represented by randomizing body parameters, actuator noise, contact properties, and sensory latency [147,148]. A principle that persists across these perturbations is more likely to be a transferable design constraint than a property of one particular dataset version.

The appropriate baselines depend on the claim. For a topology claim, use degree-matched, community-matched, and shuffled graphs [142,143]. For a spiking claim, compare with rate and recurrent models trained under comparable optimization budgets [96]. For a body-interface claim, compare learned adapters, hand-designed adapters, and direct actuation. For a biological interpretation, include targeted perturbation predictions and, where available, behavioral or physiological evidence [52]. This discipline is particularly important for large models, whose capacity can mask the contribution of the connectome.

Simulation-to-real studies in legged robotics supply a second set of controls (Section 5.4). Actuator modeling and randomized dynamics address a different failure mode from online adaptation [145,151], and proprioceptive history alone can support robust locomotion, whereas a recurrent perceptive controller combines proprioception with exteroception [149,150]. None of these controllers is derived from *Drosophila* anatomy, but together they show that observation access, actuator modeling, training diversity, and online adaptation must be matched in any transfer experiment and that a claimed robustness advantage of connectome structure should be measured as a slower degradation under the stress tests of Table 6.

7. Discussion

7.1. Why the Connectome Is a Prior Rather than a Finished Controller

A digital *Drosophila* is most valuable when its anatomical detail constrains a question that simpler models cannot answer. The graph can reveal repeated routes, convergent bottlenecks, reciprocal loops, and interfaces between brain and VNC [11,22]. It also provides a common coordinate system for interventions and for comparing models across datasets [38]. These strengths make connectomics unusually useful for biomimetic engineering.

The same detail becomes a liability when it is treated as a complete specification. A synapse-resolved graph still leaves signs, strengths, delays, neuromodulatory context, developmental state, and body mechanics uncertain [13,14]. A controller that reproduces a graph but learns most of its behavior from a large task dataset may be a capable policy without showing that the graph mattered. The appropriate response is not to discard the data but to partition the claim: identify what the graph fixes, what the model assumes, and what task training estimates. Combining the connectome with targeted perturbation experiments to estimate effective connectivity is one promising way to narrow this gap [47].

This position has a general methodological precedent. Neuroscience-style analyses applied to a microprocessor of known design failed to recover its information-processing hierarchy, showing that a correct description of activity or connectivity need not reveal computation [161]. Parameter ambiguity in neural and biochemical models creates a related problem, because different parameter combinations can explain similar observations [48,98]. For connectome-based control, interventions should therefore be interpreted at the level they actually test: a model pathway may be causally necessary for the implemented task before it has been shown to be the mechanism that the animal uses.

7.2. Comparative Scope and Transfer Beyond Drosophila

Adult *Drosophila* combines dense anatomical resources with a compact body and a diverse sensorimotor repertoire, and other organisms offer useful scales as well [163]. The *Caenorhabditis elegans* wiring diagram and later whole-animal reconstructions provide a smaller setting for studying connectivity, development, and brain–body integration [164–166]. OpenWorm and data-driven worm models make the body and environment explicit rather than treating the connectome as a self-sufficient controller [167,168]. The choice of organism should follow the question being tested rather than a presumed ranking of biological systems.

Other datasets answer narrower but complementary questions. A larval *Ciona* reconstruction links a compact chordate nervous system to its effectors [169]. Serial-section EM of the whole larval zebrafish brain captures long-range organization and provides a substrate for targeted reconstruction [170]. MICrONS combines functional measurements with dense reconstruction of mouse visual cortex, and a petavoxel fragment of human cortex offers exceptional local ultrastructural detail [171,172]. Each resource supports claims at a different scale, whether local, developmental, functional, or whole-system.

Biological prediction is a separate outcome, even when a body is simulated. A virtual rodent trained to imitate natural movements produced network activity that predicted the structure of neural recordings across behaviors [173], and NeuroMechFly and FlyBody provide the corresponding *Drosophila* body platforms for sensorimotor and locomotion studies [17,54]. Agreement with neural activity is a valuable additional target; engineering utility, biological prediction, and anatomical correspondence nevertheless remain distinct outcomes, and each requires its own evidence.

7.3. A Practical Research Program for Embodied Intelligence

The literature suggests a staged program. Begin with a small mechanism whose inputs and outputs can be interpreted, such as a recurrent navigation module or a sparse associative module [102,115]. Couple it to a body simulator and test it against matched graph baselines [17]. Expand the neural graph only when the added anatomical coverage answers a new control question, such as brain–VNC coordination or multi-limb behavior [11, 35]. Finally, evaluate transfer across bodies and environments with uncertainty-aware ablations. This sequence follows the biorobotic tradition of using physical models to test biological hypotheses [132,134], and it keeps biological detail tied to an engineering decision.

The same program implies a division of labor between data and models. Connectomics supplies structural hypotheses and anatomical indices; physiology and behavior constrain dynamics and signs; simulation exposes body-level consequences; and machine learning estimates parameters and tests adaptation. The result is not a single digital *Drosophila* but a family of models that share a traceable structural prior and differ in their assumptions about dynamics and embodiment.

7.4. Open Challenges

Several gaps remain before a complete, experimentally calibrated brain–body controller can be built. The adult resources differ in sex, specimen, anatomical coverage, dataset version, proofreading, and cell-type annotation [15,24,38], so models that span datasets depend on cell-type matching and on the reproducibility practices of Section 3.4. The sensory periphery, the muscles, gap junctions, and neuromodulatory state are only partly represented or absent (Section 2.3). Large-scale graph models rely on approximations that have been validated for selected pathways rather than for the whole system [47,52]. Transferring a *Drosophila* topology to a robot also changes the sensor statistics, body morphology, actuator dynamics, and task distribution, so claims of general biomimicry should remain narrower than claims of engineering usefulness.

Shared infrastructure would accelerate progress on these gaps. A shared, machine-readable table that records the anatomical coverage, annotation confidence, and benchmark performance of each dataset version would let model builders choose datasets as they now choose software libraries [34,70]. Closed-loop benchmarks built on open body simulators, including conventional controllers among the baselines and the sim-to-real stress tests of Table 6, would make matched comparisons between connectomic and conventional controllers routine [17,54]. Perturbation experiments designed with the help of the connectome would, in turn, supply the dynamical constraints that anatomy alone cannot provide [47].

8. Conclusions

Adult *Drosophila* connectomics has moved from local circuit reconstructions to synapse-resolved maps of the whole brain, the VNC, and, in BANC, the two together. These maps are estimates that keep improving: they are produced by imaging, automated segmentation, synapse partner assignment, and human proofreading, they are corrected and reissued over time, and any errors that remain propagate directly into a controller built on them. What a connectome fixes is the set of possible interactions between identified neurons and cell types. Synaptic signs and strengths, neuromodulatory state, motor decoding, and body mechanics must be supplied by physiology, modeling, or learning.

For embodied control, the connectome is therefore best used as a structural prior, and three routes follow from this view. Extracting a circuit principle, such as ring-attractor heading estimation or sparse associative learning, gives the most portable result. Embedding a reconstructed module, such as a connectome-constrained visual network, preserves an identifiable mechanism while its interfaces are adapted to a new body. Using a whole connectome as the controller topology provides the strongest structural test but depends most on the biology that is still missing. The first two routes are currently the best supported; the third has only begun to be explored in simulated locomotion.

Three practices would make results along any of these routes comparable. First, a study should state which properties are fixed by anatomy, which are estimated from physiology, and which are learned for the task, together with the exact dataset version used. Second, every topology claim needs matched baselines: degree-preserving and community-matched graphs, rate and spiking variants trained under the same budget, and alternative sensor and motor adapters. Third, controllers should be evaluated against conventional baselines under sensor noise, delay, friction change, body perturbation, and changes in morphology, with anatomical and dynamical uncertainty carried through to the results. Throughout, experimentally validated findings should be kept distinct from computational predictions and engineering proposals because simulated success alone does not establish biological accuracy.

Sparse modular communication, recurrent state estimation, hierarchical motor control, selective plasticity, and body–controller co-design are the five most promising candidate design principles for transfer because they describe relationships rather than species-specific structures; anatomically indexed intervention is a sixth, methodological principle for testing them. Their support from *Drosophila* data differs: recurrent state estimation and selective plasticity are the most strongly *Drosophila*-derived, whereas the others were established elsewhere and are refined by connectomic constraints. Table 9 states a falsifiable prediction for each. Brain–VNC connectomes, perturbation experiments that estimate effective connectivity, and shared closed-loop benchmarks on open body simulators now provide the means to test them. If these principles survive such tests, digital *Drosophila* will serve less as a controller to copy than as a source of verified design rules for embodied agents.

Author Contributions: Conceptualization, methodology, software, investigation, data curation, formal analysis, and visualization, W.J.; writing—original draft, W.J.; validation, resources, writing—review and editing, supervision, and funding acquisition, L.X. All authors have read and agreed to the published version of the manuscript.

Funding: This work was supported by the National Natural Science Foundation of China (Grant No. 62373286).

Institutional Review Board Statement: Not applicable.

Informed Consent Statement: Not applicable.

Data Availability Statement: No new data were created or analyzed in this study. Data sharing is not applicable to this article.

Conflicts of Interest: The authors declare no competing interests.

Abbreviations

The following abbreviations are used in this manuscript:

ATUM	Automated tape-collecting ultramicrotomy
BANC	Brain And Nerve Cord connectome
CAVE	Connectome Annotation Versioning Engine
CPG	Central pattern generator
EM	Electron microscopy
FAFB	Full Adult Fly Brain
FANC	Female Adult Nerve Cord
FIB-SEM	Focused ion beam scanning electron microscopy
LIF	Leaky integrate-and-fire
MANC	Male Adult Nerve Cord
MLP	Multilayer perceptron
MPC	Model-predictive control
RL	Reinforcement learning
RNN	Recurrent neural network
ssTEM	Serial-section transmission electron microscopy
VNC	Ventral nerve cord

References

1. Pfeifer, R.; Lungarella, M.; Iida, F. Self-Organization, Embodiment, and Biologically Inspired Robotics. *Science* **2007**, *318*, 1088–1093. [CrossRef]
2. Liu, H.; Guo, D.; Cangelosi, A. Embodied Intelligence: A Synergy of Morphology, Action, Perception and Learning. *ACM Comput. Surv.* **2025**, *57*, 1–36. [CrossRef]
3. Chiel, H.J.; Beer, R.D. The brain has a body: Adaptive behavior emerges from interactions of nervous system, body and environment. *Trends Neurosci.* **1997**, *20*, 553–557. [CrossRef]
4. Dickinson, M.H.; Farley, C.T.; Full, R.J.; Koehl, M.A.R.; Kram, R.; Lehman, S. How Animals Move: An Integrative View. *Science* **2000**, *288*, 100–106. [CrossRef]
5. Chittka, L.; Niven, J. Are Bigger Brains Better? *Curr. Biol.* **2009**, *19*, R995–R1008. [CrossRef]
6. Webb, B. Robots with insect brains. *Science* **2020**, *368*, 244–245. [CrossRef]
7. Dorkenwald, S.; Matsliah, A.; Sterling, A.R.; Schlegel, P.; Yu, S.c.; McKellar, C.E.; Lin, A.; Costa, M.; Eichler, K.; Yin, Y.; et al. Neuronal wiring diagram of an adult brain. *Nature* **2024**, *634*, 124–138. [CrossRef]
8. Olsen, S.R.; Wilson, R.I. Cracking neural circuits in a tiny brain: New approaches for understanding the neural circuitry of Drosophila. *Trends Neurosci.* **2008**, *31*, 512–520. [CrossRef]
9. Zheng, Z.; Lauritzen, J.S.; Perlman, E.; Robinson, C.G.; Nichols, M.; Milkie, D.; Torrens, O.; Price, J.; Fisher, C.B.; Sharifi, N.; et al. A Complete Electron Microscopy Volume of the Brain of Adult Drosophila melanogaster. *Cell* **2018**, *174*, 730–743.e22. [CrossRef]
10. Dorkenwald, S.; McKellar, C.E.; Macrina, T.; Kemnitz, N.; Lee, K.; Lu, R.; Wu, J.; Popovych, S.; Mitchell, E.; Nehoran, B.; et al. FlyWire: Online community for whole-brain connectomics. *Nat. Methods* **2022**, *19*, 119–128. [CrossRef]
11. Bates, A.S.; Phelps, J.S.; Kim, M.; Yang, H.H.; Matsliah, A.; Ajabi, Z.; Perlman, E.; Delgado, K.M.; Osman, M.A.M.; Salmon, C.K.; et al. Distributed control circuits across a brain-and-cord connectome. *Nature* **2026**, *656*, 957–970. [CrossRef]
12. Litwin-Kumar, A.; Turaga, S.C. Constraining computational models using electron microscopy wiring diagrams. *Curr. Opin. Neurobiol.* **2019**, *58*, 94–100. [CrossRef]
13. Bargmann, C.I.; Marder, E. From the connectome to brain function. *Nat. Methods* **2013**, *10*, 483–490. [CrossRef]
14. Marder, E. Neuromodulation of Neuronal Circuits: Back to the Future. *Neuron* **2012**, *76*, 1–11. [CrossRef]
15. Takemura, S.y.; Hayworth, K.J.; Huang, G.B.; Januszewski, M.; Lu, Z.; Marin, E.C.; Preibisch, S.; Xu, C.S.; Bogovic, J.; Champion, A.S.; et al. A Connectome of the Male Drosophila Ventral Nerve Cord. *BioRxiv* **2023**. [CrossRef]
16. Jin, Z.; Zhu, Y.; Zhang, C.; Sui, Y. Whole-Brain Connectomic Graph Model Enables Whole-Body Locomotion Control in Fruit Fly. *arXiv* **2026**, arXiv:2602.17997. [CrossRef]
17. Wang-Chen, S.; Stimpfling, V.A.; Lam, T.K.C.; Özdil, P.G.; Genoud, L.; Hurtak, F.; Ramdya, P. NeuroMechFly v2: Simulating embodied sensorimotor control in adult Drosophila. *Nat. Methods* **2024**, *21*, 2353–2362. [CrossRef]
18. Tuthill, J.C.; Wilson, R.I. Mechanosensation and Adaptive Motor Control in Insects. *Curr. Biol.* **2016**, *26*, R1022–R1038. [CrossRef]

19. Mamiya, A.; Gurung, P.; Tuthill, J.C. Neural Coding of Leg Proprioception in Drosophila. *Neuron* **2018**, *100*, 636–650.e6. [CrossRef]
20. Plaza, S.M.; Scheffer, L.K.; Chklovskii, D.B. Toward large-scale connectome reconstructions. *Curr. Opin. Neurobiol.* **2014**, *25*, 201–210. [CrossRef]
21. Lichtman, J.W.; Pfister, H.; Shavit, N. The big data challenges of connectomics. *Nat. Neurosci.* **2014**, *17*, 1448–1454. [CrossRef]
22. Lin, A.; Yang, R.; Dorkenwald, S.; Matsliah, A.; Sterling, A.R.; Schlegel, P.; Yu, S.C.; McKellar, C.E.; Costa, M.; Eichler, K.; et al. Network statistics of the whole-brain connectome of Drosophila. *Nature* **2024**, *634*, 153–165. [CrossRef]
23. Phelps, J.S.; Hildebrand, D.G.C.; Graham, B.J.; Kuan, A.T.; Thomas, L.A.; Nguyen, T.M.; Buhmann, J.; Azevedo, A.W.; Sustar, A.; Agrawal, S.; et al. Reconstruction of motor control circuits in adult Drosophila using automated transmission electron microscopy. *Cell* **2021**, *184*, 759–774.e18. [CrossRef]
24. Azevedo, A.; Lesser, E.; Phelps, J.S.; Mark, B.; Elabbady, L.; Kuroda, S.; Sustar, A.; Moussa, A.; Khandelwal, A.; Dallmann, C.J.; et al. Connectomic reconstruction of a female Drosophila ventral nerve cord. *Nature* **2024**, *631*, 360–368. [CrossRef]
25. Scheffer, L.K.; Xu, C.S.; Januszewski, M.; Lu, Z.; Takemura, S.y.; Hayworth, K.J.; Huang, G.B.; Shinomiya, K.; Maitlin-Shepard, J.; Berg, S.; et al. A connectome and analysis of the adult Drosophila central brain. *eLife* **2020**, *9*, e57443. [CrossRef]
26. Hulse, B.K.; Haberkern, H.; Franconville, R.; Turner-Evans, D.; Takemura, S.y.; Wolff, T.; Noorman, M.; Dreher, M.; Dan, C.; Parekh, R.; et al. A connectome of the Drosophila central complex reveals network motifs suitable for flexible navigation and context-dependent action selection. *eLife* **2021**, *10*, e66039. [CrossRef]
27. Li, F.; Lindsey, J.W.; Marin, E.C.; Otto, N.; Dreher, M.; Dempsey, G.; Stark, I.; Bates, A.S.; Pleijzier, M.W.; Schlegel, P.; et al. The connectome of the adult Drosophila mushroom body provides insights into function. *eLife* **2020**, *9*, e62576. [CrossRef]
28. Briggman, K.L.; Bock, D.D. Volume electron microscopy for neuronal circuit reconstruction. *Curr. Opin. Neurobiol.* **2012**, *22*, 154–161. [CrossRef]
29. Peddie, C.J.; Genoud, C.; Kreshuk, A.; Meechan, K.; Micheva, K.D.; Narayan, K.; Pape, C.; Parton, R.G.; Schieber, N.L.; Schwab, Y.; et al. Volume electron microscopy. *Nat. Rev. Methods Prim.* **2022**, *2*, 51. Correction in *Nat. Rev. Methods Prim.* **2022**, *2*, 72. [CrossRef]
30. Harris, K.M.; Perry, E.; Bourne, J.; Feinberg, M.; Ostroff, L.; Hurlburt, J. Uniform Serial Sectioning for Transmission Electron Microscopy. *J. Neurosci.* **2006**, *26*, 12101–12103. [CrossRef]
31. Bock, D.D.; Lee, W.C.A.; Kerlin, A.M.; Andermann, M.L.; Hood, G.; Wetzel, A.W.; Yurgenson, S.; Soucy, E.R.; Kim, H.S.; Reid, R.C. Network anatomy and in vivo physiology of visual cortical neurons. *Nature* **2011**, *471*, 177–182. [CrossRef]
32. Knott, G.; Marchman, H.; Wall, D.; Lich, B. Serial Section Scanning Electron Microscopy of Adult Brain Tissue Using Focused Ion Beam Milling. *J. Neurosci.* **2008**, *28*, 2959–2964. [CrossRef]
33. Xu, C.S.; Hayworth, K.J.; Lu, Z.; Grob, P.; Hassan, A.M.; García-Cerdán, J.G.; Niyogi, K.K.; Nogales, E.; Weinberg, R.J.; Hess, H.F. Enhanced FIB-SEM systems for large-volume 3D imaging. *eLife* **2017**, *6*, e25916. [CrossRef]
34. Dorkenwald, S.; Schneider-Mizell, C.M.; Brittain, D.; Halageri, A.; Jordan, C.; Kemnitz, N.; Castro, M.A.; Silversmith, W.; Maitin-Shephard, J.; Troidl, J.; et al. CAVE: Connectome Annotation Versioning Engine. *Nat. Methods* **2025**, *22*, 1112–1120. [CrossRef]
35. Cheong, H.S.; Eichler, K.; Stürner, T.; Asinof, S.K.; Champion, A.S.; Marin, E.C.; Oram, T.B.; Sumathipala, M.; Venkatasubramanian, L.; Namiki, S.; et al. Organization of circuits linking descending input to motor output in the Drosophila Male Adult Nerve Cord connectome. *eLife* **2026**, *13*, RP96084. [CrossRef]
36. Nern, A.; Loesche, F.; Takemura, S.Y.; Burnett, L.E.; Dreher, M.; Gruntman, E.; Hoeller, J.; Huang, G.B.; Januszewski, M.; Klapoetke, N.C.; et al. Connectome-driven neural inventory of a complete visual system. *Nature* **2025**, *641*, 1225–1237. [CrossRef]
37. Winding, M.; Pedigo, B.D.; Barnes, C.L.; Patsolic, H.G.; Park, Y.; Kazimiers, T.; Fushiki, A.; Andrade, I.V.; Khandelwal, A.; Valdes-Aleman, J.; et al. The connectome of an insect brain. *Science* **2023**, *379*, eadd9330. [CrossRef]
38. Schlegel, P.; Yin, Y.; Bates, A.S.; Dorkenwald, S.; Eichler, K.; Brooks, P.; Han, D.S.; Gkantia, M.; dos Santos, M.; Munnelly, E.J.; et al. Whole-brain annotation and multi-connectome cell typing of Drosophila. *Nature* **2024**, *634*, 139–152. [CrossRef]
39. Stürner, T.; Brooks, P.; Serratosa Capdevila, L.; Morris, B.J.; Javier, A.; Fang, S.; Gkantia, M.; Cachero, S.; Beckett, I.R.; Marin, E.C.; et al. Comparative connectomics of Drosophila descending and ascending neurons. *Nature* **2025**, *643*, 158–172. [CrossRef]
40. Buhmann, J.; Sheridan, A.; Malin-Mayor, C.; Schlegel, P.; Gerhard, S.; Kazimiers, T.; Krause, R.; Nguyen, T.M.; Heinrich, L.; Lee, W.C.A.; et al. Automatic detection of synaptic partners in a whole-brain Drosophila electron microscopy data set. *Nat. Methods* **2021**, *18*, 771–774. [CrossRef]
41. Milo, R.; Shen-Orr, S.; Itzkovitz, S.; Kashtan, N.; Chklovskii, D.; Alon, U. Network Motifs: Simple Building Blocks of Complex Networks. *Science* **2002**, *298*, 824–827. [CrossRef]
42. Takemura, S.y.; Bharioke, A.; Lu, Z.; Nern, A.; Vitaladevuni, S.; Rivlin, P.K.; Katz, W.T.; Olbris, D.J.; Plaza, S.M.; Winston, P.; et al. A visual motion detection circuit suggested by Drosophila connectomics. *Nature* **2013**, *500*, 175–181. [CrossRef]
43. Kopell, N.J.; Gritton, H.J.; Whittington, M.A.; Kramer, M.A. Beyond the Connectome: The Dynome. *Neuron* **2014**, *83*, 1319–1328. [CrossRef]
44. Zucker, R.S.; Regehr, W.G. Short-Term Synaptic Plasticity. *Annu. Rev. Physiol.* **2002**, *64*, 355–405. [CrossRef]

45. Liu, W.W.; Wilson, R.I. Glutamate is an inhibitory neurotransmitter in the Drosophila olfactory system. *Proc. Natl. Acad. Sci. USA* **2013**, *110*, 10294–10299. [CrossRef]
46. Gutierrez, G.J.; O'Leary, T.; Marder, E. Multiple Mechanisms Switch an Electrically Coupled, Synaptically Inhibited Neuron between Competing Rhythmic Oscillators. *Neuron* **2013**, *77*, 845–858. [CrossRef]
47. Pospisil, D.A.; Aragon, M.J.; Dorkenwald, S.; Matsliah, A.; Sterling, A.R.; Schlegel, P.; Yu, S.c.; McKellar, C.E.; Costa, M.; Eichler, K.; et al. The fly connectome reveals a path to the effectome. *Nature* **2024**, *634*, 201–209. [CrossRef]
48. Prinz, A.A.; Bucher, D.; Marder, E. Similar network activity from disparate circuit parameters. *Nat. Neurosci.* **2004**, *7*, 1345–1352. [CrossRef]
49. Marder, E.; Goaillard, J.M. Variability, compensation and homeostasis in neuron and network function. *Nat. Rev. Neurosci.* **2006**, *7*, 563–574. [CrossRef]
50. Lazar, A.A.; Liu, T.; Turkcan, M.K.; Zhou, Y. Accelerating with FlyBrainLab the discovery of the functional logic of the Drosophila brain in the connectomic and synaptomic era. *eLife* **2021**, *10*, e62362. [CrossRef]
51. Lappalainen, J.K.; Tschopp, F.D.; Prakhya, S.; McGill, M.; Nern, A.; Shinomiya, K.; Takemura, S.y.; Gruntman, E.; Macke, J.H.; Turaga, S.C. Connectome-constrained networks predict neural activity across the fly visual system. *Nature* **2024**, *634*, 1132–1140. [CrossRef]
52. Shiu, P.K.; Sterne, G.R.; Spiller, N.; Franconville, R.; Sandoval, A.; Zhou, J.; Simha, N.; Kang, C.H.; Yu, S.; Kim, J.S.; et al. A Drosophila computational brain model reveals sensorimotor processing. *Nature* **2024**, *634*, 210–219. [CrossRef]
53. Lobato-Rios, V.; Ramalingasetty, S.T.; Özdil, P.G.; Arreguit, J.; Ijspeert, A.J.; Ramdya, P. NeuroMechFly, a neuromechanical model of adult Drosophila melanogaster. *Nat. Methods* **2022**, *19*, 620–627. [CrossRef]
54. Vaxenburg, R.; Siwanowicz, I.; Merel, J.; Robie, A.A.; Morrow, C.; Novati, G.; Stefanidi, Z.; Both, G.J.; Card, G.M.; Reiser, M.B.; et al. Whole-body physics simulation of fruit fly locomotion. *Nature* **2025**, *643*, 1312–1320. [CrossRef]
55. Eckstein, N.; Bates, A.S.; Champion, A.; Du, M.; Yin, Y.; Schlegel, P.; Lu, A.K.Y.; Rymer, T.; Finley-May, S.; Paterson, T.; et al. Neurotransmitter classification from electron microscopy images at synaptic sites in Drosophila melanogaster. *Cell* **2024**, *187*, 2574–2594.e23. [CrossRef]
56. Ammer, G.; Vieira, R.M.; Fendl, S.; Borst, A. Anatomical distribution and functional roles of electrical synapses in Drosophila. *Curr. Biol.* **2022**, *32*, 2022–2036.e4. [CrossRef]
57. Kornfeld, J.; Denk, W. Progress and remaining challenges in high-throughput volume electron microscopy. *Curr. Opin. Neurobiol.* **2018**, *50*, 261–267. [CrossRef]
58. Micheva, K.D.; Smith, S.J. Array Tomography: A New Tool for Imaging the Molecular Architecture and Ultrastructure of Neural Circuits. *Neuron* **2007**, *55*, 25–36. [CrossRef]
59. Hayworth, K.J.; Morgan, J.L.; Schalek, R.; Berger, D.R.; Hildebrand, D.G.C.; Lichtman, J.W. Imaging ATUM ultrathin section libraries with WaferMapper: A multi-scale approach to EM reconstruction of neural circuits. *Front. Neural Circuits* **2014**, *8*, 68. [CrossRef]
60. Saalfeld, S.; Fetter, R.; Cardona, A.; Tomancak, P. Elastic volume reconstruction from series of ultra-thin microscopy sections. *Nat. Methods* **2012**, *9*, 717–720. [CrossRef]
61. Hanslovsky, P.; Bogovic, J.A.; Saalfeld, S. Image-based correction of continuous and discontinuous non-planar axial distortion in serial section microscopy. *Bioinformatics* **2017**, *33*, 1379–1386. [CrossRef]
62. Mahalingam, G.; Torres, R.; Kapner, D.; Trautman, E.T.; Fliss, T.; Seshamani, S.; Perlman, E.; Young, R.; Kinn, S.; Buchanan, J.; et al. A scalable and modular automated pipeline for stitching of large electron microscopy datasets. *eLife* **2022**, *11*, e76534. [CrossRef]
63. Denk, W.; Horstmann, H. Serial Block-Face Scanning Electron Microscopy to Reconstruct Three-Dimensional Tissue Nanostructure. *PLoS Biol.* **2004**, *2*, e329. [CrossRef]
64. Hayworth, K.J.; Xu, C.S.; Lu, Z.; Knott, G.W.; Fetter, R.D.; Tapia, J.C.; Lichtman, J.W.; Hess, H.F. Ultrastructurally smooth thick partitioning and volume stitching for large-scale connectomics. *Nat. Methods* **2015**, *12*, 319–322. [CrossRef]
65. Eberle, A.L.; Mikula, S.; Schalek, R.; Lichtman, J.; Knothe Tate, M.L.; Zeidler, D. High-resolution, high-throughput imaging with a multibeam scanning electron microscope. *J. Microsc.* **2015**, *259*, 114–120. [CrossRef]
66. Yin, W.; Brittain, D.; Borseth, J.; Scott, M.E.; Williams, D.; Perkins, J.; Own, C.S.; Murfitt, M.; Torres, R.M.; Kapner, D.; et al. A petascale automated imaging pipeline for mapping neuronal circuits with high-throughput transmission electron microscopy. *Nat. Commun.* **2020**, *11*, 4949. [CrossRef]
67. Mikula, S.; Denk, W. High-resolution whole-brain staining for electron microscopic circuit reconstruction. *Nat. Methods* **2015**, *12*, 541–546. [CrossRef]
68. Hua, Y.; Laserstein, P.; Helmstaedter, M. Large-volume en-bloc staining for electron microscopy-based connectomics. *Nat. Commun.* **2015**, *6*, 7923. [CrossRef]
69. Lu, Z.; Xu, C.S.; Hayworth, K.J.; Pang, S.; Shinomiya, K.; Plaza, S.M.; Scheffer, L.K.; Rubin, G.M.; Hess, H.F.; Rivlin, P.K.; et al. En bloc preparation of Drosophila brains enables high-throughput FIB-SEM connectomics. *Front. Neural Circuits* **2022**, *16*, 917251. [CrossRef]

70. Plaza, S.M.; Clements, J.; Dolafi, T.; Umayam, L.; Neubarth, N.N.; Scheffer, L.K.; Berg, S. neuPrint: An open access tool for EM connectomics. *Front. Neuroinform.* **2022**, *16*, 896292. [CrossRef]
71. Januszewski, M.; Kornfeld, J.; Li, P.H.; Pope, A.; Blakely, T.; Lindsey, L.; Maitin-Shepard, J.; Tyka, M.; Denk, W.; Jain, V. High-precision automated reconstruction of neurons with flood-filling networks. *Nat. Methods* **2018**, *15*, 605–610. [CrossRef]
72. Lee, K.; Lu, R.; Luther, K.; Seung, H.S. Learning and Segmenting Dense Voxel Embeddings for 3D Neuron Reconstruction. *IEEE Trans. Med. Imaging* **2021**, *40*, 3801–3811. [CrossRef]
73. Heinrich, L.; Bennett, D.; Ackerman, D.; Park, W.; Bogovic, J.; Eckstein, N.; Petruncio, A.; Clements, J.; Pang, S.; Xu, C.S.; et al. Whole-cell organelle segmentation in volume electron microscopy. *Nature* **2021**, *599*, 141–146. [CrossRef]
74. Turaga, S.C.; Murray, J.F.; Jain, V.; Roth, F.; Helmstaedter, M.; Briggman, K.; Denk, W.; Seung, H.S. Convolutional Networks Can Learn to Generate Affinity Graphs for Image Segmentation. *Neural Comput.* **2010**, *22*, 511–538. [CrossRef]
75. Çiçek, O.; Abdulkadir, A.; Lienkamp, S.S.; Brox, T.; Ronneberger, O. 3D U-Net: Learning Dense Volumetric Segmentation from Sparse Annotation. In *Proceedings of the Medical Image Computing and Computer-Assisted Intervention–MICCAI 2016*; Lecture notes in computer science; Springer International Publishing: Berlin/Heidelberg, Germany, 2016; pp. 424–432. [CrossRef]
76. Funke, J.; Tschopp, F.; Grisaitis, W.; Sheridan, A.; Singh, C.; Saalfeld, S.; Turaga, S.C. Large Scale Image Segmentation with Structured Loss Based Deep Learning for Connectome Reconstruction. *IEEE Trans. Pattern Anal. Mach. Intell.* **2019**, *41*, 1669–1680. [CrossRef]
77. Sheridan, A.; Nguyen, T.M.; Deb, D.; Lee, W.C.A.; Saalfeld, S.; Turaga, S.C.; Manor, U.; Funke, J. Local shape descriptors for neuron segmentation. *Nat. Methods* **2023**, *20*, 295–303. [CrossRef]
78. Arganda-Carreras, I.; Turaga, S.C.; Berger, D.R.; Cireşan, D.; Giusti, A.; Gambardella, L.M.; Schmidhuber, J.; Laptev, D.; Dwivedi, S.; Buhmann, J.M.; et al. Crowdsourcing the creation of image segmentation algorithms for connectomics. *Front. Neuroanat.* **2015**, *9*, 142. [CrossRef]
79. Reilly, E.P.; Garretson, J.S.; Gray Roncal, W.R.; Kleissas, D.M.; Wester, B.A.; Chevillet, M.A.; Roos, M.J. Neural Reconstruction Integrity: A Metric for Assessing the Connectivity Accuracy of Reconstructed Neural Networks. *Front. Neuroinform.* **2018**, *12*, 74. [CrossRef]
80. Shit, S.; Paetzold, J.C.; Sekuboyina, A.; Ezhov, I.; Unger, A.; Zhylka, A.; Pluim, J.P.W.; Bauer, U.; Menze, B.H. clDice - a Novel Topology-Preserving Loss Function for Tubular Structure Segmentation. In Proceedings of the 2021 IEEE/CVF Conference on Computer Vision and Pattern Recognition (CVPR), Nashville, TN, USA, 20–25 June 2021; pp. 16555–16564. [CrossRef]
81. Celii, B.; Papadopoulos, S.; Ding, Z.; Fahey, P.G.; Wang, E.; Papadopoulos, C.; Kunin, A.B.; Patel, S.; Bae, J.A.; Bodor, A.L.; et al. NEURD offers automated proofreading and feature extraction for connectomics. *Nature* **2025**, *640*, 487–496. [CrossRef]
82. Costa, M.; Manton, J.D.; Ostrovsky, A.D.; Prohaska, S.; Jefferis, G.S.X.E. NBLAST: Rapid, Sensitive Comparison of Neuronal Structure and Construction of Neuron Family Databases. *Neuron* **2016**, *91*, 293–311. [CrossRef]
83. Saalfeld, S.; Cardona, A.; Hartenstein, V.; Tomančák, P. CATMAID: Collaborative annotation toolkit for massive amounts of image data. *Bioinformatics* **2009**, *25*, 1984–1986. [CrossRef]
84. Schneider-Mizell, C.M.; Gerhard, S.; Longair, M.; Kazimiers, T.; Li, F.; Zwart, M.F.; Champion, A.; Midgley, F.M.; Fetter, R.D.; Saalfeld, S.; et al. Quantitative neuroanatomy for connectomics in Drosophila. *eLife* **2016**, *5*, e12059. [CrossRef]
85. Boergens, K.M.; Berning, M.; Bocklisch, T.; Bräunlein, D.; Drawitsch, F.; Frohnhofen, J.; Herold, T.; Otto, P.; Rzepka, N.; Werkmeister, T.; et al. webKnossos: Efficient online 3D data annotation for connectomics. *Nat. Methods* **2017**, *14*, 691–694. [CrossRef]
86. Zhao, T.; Olbris, D.J.; Yu, Y.; Plaza, S.M. NeuTu: Software for Collaborative, Large-Scale, Segmentation-Based Connectome Reconstruction. *Front. Neural Circuits* **2018**, *12*, 101. [CrossRef]
87. Haehn, D.; Kaynig, V.; Tompkin, J.; Lichtman, J.W.; Pfister, H. Guided Proofreading of Automatic Segmentations for Connectomics. In Proceedings of the 2018 IEEE/CVF Conference on Computer Vision and Pattern Recognition, Salt Lake City, UT, USA, 18–22 June 2018; pp. 9319–9328. [CrossRef]
88. Hider, R., Jr.; Kleissas, D.; Gion, T.; Xenes, D.; Matelsky, J.; Pryor, D.; Rodriguez, L.; Johnson, E.C.; Gray-Roncal, W.; Wester, B. The Brain Observatory Storage Service and Database (BossDB): A Cloud-Native Approach for Petascale Neuroscience Discovery. *Front. Neuroinform.* **2022**, *16*, 828787. [CrossRef]
89. Bates, A.S.; Manton, J.D.; Jagannathan, S.R.; Costa, M.; Schlegel, P.; Rohlfing, T.; Jefferis, G.S. The natverse, a versatile toolbox for combining and analysing neuroanatomical data. *eLife* **2020**, *9*, e53350. [CrossRef]
90. Bogovic, J.A.; Otsuna, H.; Heinrich, L.; Ito, M.; Jeter, J.; Meissner, G.; Nern, A.; Colonell, J.; Malkesman, O.; Ito, K.; et al. An unbiased template of the Drosophila brain and ventral nerve cord. *PLoS ONE* **2020**, *15*, e0236495. [CrossRef]
91. Hodgkin, A.L.; Huxley, A.F. A quantitative description of membrane current and its application to conduction and excitation in nerve. *J. Physiol.* **1952**, *117*, 500–544. [CrossRef]
92. Brette, R.; Gerstner, W. Adaptive Exponential Integrate-and-Fire Model as an Effective Description of Neuronal Activity. *J. Neurophysiol.* **2005**, *94*, 3637–3642. [CrossRef]
93. Dasgupta, S.; Stevens, C.F.; Navlakha, S. A neural algorithm for a fundamental computing problem. *Science* **2017**, *358*, 793–796. [CrossRef]

94. Shen, Y.; Dasgupta, S.; Navlakha, S. Reducing Catastrophic Forgetting With Associative Learning: A Lesson From Fruit Flies. *Neural Comput.* **2023**, *35*, 1797–1819. [CrossRef]
95. Lechner, M.; Hasani, R.; Amini, A.; Henzinger, T.A.; Rus, D.; Grosu, R. Neural circuit policies enabling auditable autonomy. *Nat. Mach. Intell.* **2020**, *2*, 642–652. [CrossRef]
96. Neftci, E.O.; Mostafa, H.; Zenke, F. Surrogate Gradient Learning in Spiking Neural Networks: Bringing the Power of Gradient-Based Optimization to Spiking Neural Networks. *IEEE Signal Process. Mag.* **2019**, *36*, 51–63. [CrossRef]
97. Song, H.F.; Yang, G.R.; Wang, X.J. Training Excitatory-Inhibitory Recurrent Neural Networks for Cognitive Tasks: A Simple and Flexible Framework. *PLoS Comput. Biol.* **2016**, *12*, e1004792. [CrossRef]
98. Gutenkunst, R.N.; Waterfall, J.J.; Casey, F.P.; Brown, K.S.; Myers, C.R.; Sethna, J.P. Universally Sloppy Parameter Sensitivities in Systems Biology Models. *PLoS Comput. Biol.* **2007**, *3*, e189. [CrossRef]
99. Cohn, R.; Morantte, I.; Ruta, V. Coordinated and Compartmentalized Neuromodulation Shapes Sensory Processing in Drosophila. *Cell* **2015**, *163*, 1742–1755. [CrossRef]
100. Aso, Y.; Rubin, G.M. Dopaminergic neurons write and update memories with cell-type-specific rules. *eLife* **2016**, *5*, e16135. [CrossRef]
101. Seelig, J.D.; Jayaraman, V. Neural dynamics for landmark orientation and angular path integration. *Nature* **2015**, *521*, 186–191. [CrossRef]
102. Kim, S.S.; Rouault, H.; Druckmann, S.; Jayaraman, V. Ring attractor dynamics in the Drosophila central brain. *Science* **2017**, *356*, 849–853. [CrossRef]
103. Turner-Evans, D.; Wegener, S.; Rouault, H.; Franconville, R.; Wolff, T.; Seelig, J.D.; Druckmann, S.; Jayaraman, V. Angular velocity integration in a fly heading circuit. *eLife* **2017**, *6*, e23496. [CrossRef]
104. Green, J.; Adachi, A.; Shah, K.K.; Hirokawa, J.D.; Magani, P.S.; Maimon, G. A neural circuit architecture for angular integration in Drosophila. *Nature* **2017**, *546*, 101–106. [CrossRef]
105. Zhang, K. Representation of spatial orientation by the intrinsic dynamics of the head-direction cell ensemble: A theory. *J. Neurosci.* **1996**, *16*, 2112–2126. [CrossRef]
106. Lyu, C.; Abbott, L.F.; Maimon, G. Building an allocentric travelling direction signal via vector computation. *Nature* **2022**, *601*, 92–97. [CrossRef]
107. Lu, J.; Behbahani, A.H.; Hamburg, L.; Westeinde, E.A.; Dawson, P.M.; Lyu, C.; Maimon, G.; Dickinson, M.H.; Druckmann, S.; Wilson, R.I. Transforming representations of movement from body- to world-centric space. *Nature* **2022**, *601*, 98–104. [CrossRef]
108. Stone, T.; Webb, B.; Adden, A.; Weddig, N.B.; Honkanen, A.; Templin, R.; Wcislo, W.; Scimeca, L.; Warrant, E.; Heinze, S. An Anatomically Constrained Model for Path Integration in the Bee Brain. *Curr. Biol.* **2017**, *27*, 3069–3085.e11. [CrossRef]
109. Maisak, M.S.; Haag, J.; Ammer, G.; Serbe, E.; Meier, M.; Leonhardt, A.; Schilling, T.; Bahl, A.; Rubin, G.M.; Nern, A.; et al. A directional tuning map of Drosophila elementary motion detectors. *Nature* **2013**, *500*, 212–216. [CrossRef]
110. Strother, J.A.; Wu, S.T.; Wong, A.M.; Nern, A.; Rogers, E.M.; Le, J.Q.; Rubin, G.M.; Reiser, M.B. The Emergence of Directional Selectivity in the Visual Motion Pathway of Drosophila. *Neuron* **2017**, *94*, 168–182.e10. [CrossRef]
111. Takemura, S.y.; Nern, A.; Chklovskii, D.B.; Scheffer, L.K.; Rubin, G.M.; Meinertzhagen, I.A. The comprehensive connectome of a neural substrate for 'ON' motion detection in Drosophila. *eLife* **2017**, *6*, e24394. [CrossRef]
112. Arenz, A.; Drews, M.S.; Richter, F.G.; Ammer, G.; Borst, A. The Temporal Tuning of the Drosophila Motion Detectors Is Determined by the Dynamics of Their Input Elements. *Curr. Biol.* **2017**, *27*, 929–944. [CrossRef]
113. Eichler, K.; Li, F.; Litwin-Kumar, A.; Park, Y.; Andrade, I.; Schneider-Mizell, C.M.; Saumweber, T.; Huser, A.; Eschbach, C.; Gerber, B.; et al. The complete connectome of a learning and memory centre in an insect brain. *Nature* **2017**, *548*, 175–182. [CrossRef]
114. Lin, A.C.; Bygrave, A.M.; de Calignon, A.; Lee, T.; Miesenböck, G. Sparse, decorrelated odor coding in the mushroom body enhances learned odor discrimination. *Nat. Neurosci.* **2014**, *17*, 559–568. [CrossRef]
115. Aso, Y.; Hattori, D.; Yu, Y.; Johnston, R.M.; Iyer, N.A.; Ngo, T.T.; Dionne, H.; Abbott, L.F.; Axel, R.; Tanimoto, H.; et al. The neuronal architecture of the mushroom body provides a logic for associative learning. *eLife* **2014**, *3*, e04577. [CrossRef]
116. Hige, T.; Aso, Y.; Rubin, G.M.; Turner, G.C. Plasticity-driven individualization of olfactory coding in mushroom body output neurons. *Nature* **2015**, *526*, 258–262. [CrossRef]
117. Bennett, J.E.M.; Philippides, A.; Nowotny, T. Learning with reinforcement prediction errors in a model of the Drosophila mushroom body. *Nat. Commun.* **2021**, *12*, 2569. [CrossRef]
118. Braun, J.; Hurtak, F.; Wang-Chen, S.; Ramdya, P. Descending networks transform command signals into population motor control. *Nature* **2024**, *630*, 686–694. [CrossRef]
119. Merel, J.; Botvinick, M.; Wayne, G. Hierarchical motor control in mammals and machines. *Nat. Commun.* **2019**, *10*, 5489. [CrossRef]
120. Bidaye, S.S.; Machacek, C.; Wu, Y.; Dickson, B.J. Neuronal Control of Drosophila Walking Direction. *Science* **2014**, *344*, 97–101. [CrossRef]

121. Cande, J.; Namiki, S.; Qiu, J.; Korff, W.; Card, G.M.; Shaevitz, J.W.; Stern, D.L.; Berman, G.J. Optogenetic dissection of descending behavioral control in Drosophila. *eLife* **2018**, *7*, e34275. [CrossRef]
122. Namiki, S.; Dickinson, M.H.; Wong, A.M.; Korff, W.; Card, G.M. The functional organization of descending sensory-motor pathways in Drosophila. *eLife* **2018**, *7*, e34272. [CrossRef]
123. Agrawal, S.; Dickinson, E.S.; Sustar, A.; Gurung, P.; Shepherd, D.; Truman, J.W.; Tuthill, J.C. Central processing of leg proprioception in Drosophila. *eLife* **2020**, *9*, e60299. [CrossRef]
124. Azevedo, A.W.; Dickinson, E.S.; Gurung, P.; Venkatasubramanian, L.; Mann, R.S.; Tuthill, J.C. A size principle for recruitment of Drosophila leg motor neurons. *eLife* **2020**, *9*, e56754. [CrossRef]
125. Ramdya, P.; Ijspeert, A.J. The neuromechanics of animal locomotion: From biology to robotics and back. *Sci. Robot.* **2023**, *8*, eadg0279. [CrossRef]
126. Todorov, E.; Erez, T.; Tassa, Y. MuJoCo: A physics engine for model-based control. In Proceedings of the 2012 IEEE/RSJ International Conference on Intelligent Robots and Systems, Vilamoura-Algarve, Portugal, 7–12 October 2012; pp. 5026–5033. [CrossRef]
127. McGeer, T. Passive Dynamic Walking. *Int. J. Robot. Res.* **1990**, *9*, 62–82. [CrossRef]
128. Owaki, D.; Kano, T.; Nagasawa, K.; Tero, A.; Ishiguro, A. Simple robot suggests physical interlimb communication is essential for quadruped walking. *J. R. Soc. Interface* **2013**, *10*, 20120669. [CrossRef]
129. Collins, S.; Ruina, A.; Tedrake, R.; Wisse, M. Efficient Bipedal Robots Based on Passive-Dynamic Walkers. *Science* **2005**, *307*, 1082–1085. [CrossRef]
130. Hauser, H.; Ijspeert, A.J.; Füchslin, R.M.; Pfeifer, R.; Maass, W. Towards a theoretical foundation for morphological computation with compliant bodies. *Biol. Cybern.* **2011**, *105*, 355–370. [CrossRef]
131. Ijspeert, A.J.; Crespi, A.; Ryczko, D.; Cabelguen, J.M. From Swimming to Walking with a Salamander Robot Driven by a Spinal Cord Model. *Science* **2007**, *315*, 1416–1420. [CrossRef]
132. Ijspeert, A.J. Biorobotics: Using robots to emulate and investigate agile locomotion. *Science* **2014**, *346*, 196–203. [CrossRef]
133. Gallego, G.; Delbruck, T.; Orchard, G.; Bartolozzi, C.; Taba, B.; Censi, A.; Leutenegger, S.; Davison, A.J.; Conradt, J.; Daniilidis, K.; et al. Event-Based Vision: A Survey. *IEEE Trans. Pattern Anal. Mach. Intell.* **2022**, *44*, 154–180. [CrossRef]
134. Webb, B. Can robots make good models of biological behaviour? *Behav. Brain Sci.* **2001**, *24*, 1033–1050. [CrossRef]
135. Webb, B. Using robots to model animals: A cricket test. *Robot. Auton. Syst.* **1995**, *16*, 117–134. [CrossRef]
136. Dupeyroux, J.; Serres, J.R.; Viollet, S. AntBot: A six-legged walking robot able to home like desert ants in outdoor environments. *Sci. Robot.* **2019**, *4*, eaau0307. [CrossRef]
137. Roubieu, F.L.; Serres, J.R.; Colonnier, F.; Franceschini, N.; Viollet, S.; Ruffier, F. A biomimetic vision-based hovercraft accounts for bees' complex behaviour in various corridors. *Bioinspir. Biomim.* **2014**, *9*, 036003. [CrossRef]
138. Baddeley, B.; Graham, P.; Husbands, P.; Philippides, A. A Model of Ant Route Navigation Driven by Scene Familiarity. *PLoS Comput. Biol.* **2012**, *8*, e1002336. [CrossRef]
139. Flash, T.; Hochner, B. Motor primitives in vertebrates and invertebrates. *Curr. Opin. Neurobiol.* **2005**, *15*, 660–666. [CrossRef]
140. Manoonpong, P.; Parlitz, U.; Wörgötter, F. Neural control and adaptive neural forward models for insect-like, energy-efficient, and adaptable locomotion of walking machines. *Front. Neural Circuits* **2013**, *7*, 12. [CrossRef]
141. Hwangbo, J.; Lee, J.; Dosovitskiy, A.; Bellicoso, D.; Tsounis, V.; Koltun, V.; Hutter, M. Learning agile and dynamic motor skills for legged robots. *Sci. Robot.* **2019**, *4*, eaau5872. [CrossRef]
142. Maslov, S.; Sneppen, K. Specificity and Stability in Topology of Protein Networks. *Science* **2002**, *296*, 910–913. [CrossRef]
143. Karrer, B.; Newman, M.E.J. Stochastic blockmodels and community structure in networks. *Phys. Rev. E* **2011**, *83*, 016107. [CrossRef]
144. Zhao, W.; Queralta, J.P.; Westerlund, T. Sim-to-Real Transfer in Deep Reinforcement Learning for Robotics: A Survey. In Proceedings of the 2020 IEEE Symposium Series on Computational Intelligence (SSCI), Canberra, Australia, 1–4 December 2020; pp. 737–744. [CrossRef]
145. Tan, J.; Zhang, T.; Coumans, E.; Iscen, A.; Bai, Y.; Hafner, D.; Bohez, S.; Vanhoucke, V. Sim-to-real: Learning agile locomotion for quadruped robots. *arXiv* **2018**, arXiv:1804.10332. [CrossRef]
146. Ma, K.Y.; Chirarattananon, P.; Fuller, S.B.; Wood, R.J. Controlled Flight of a Biologically Inspired, Insect-Scale Robot. *Science* **2013**, *340*, 603–607. [CrossRef]
147. Tobin, J.; Fong, R.; Ray, A.; Schneider, J.; Zaremba, W.; Abbeel, P. Domain randomization for transferring deep neural networks from simulation to the real world. In Proceedings of the 2017 IEEE/RSJ International Conference on Intelligent Robots and Systems (IROS), Vancouver, BC, Canada, 24–28 September 2017; pp. 23–30. [CrossRef]
148. Peng, X.B.; Andrychowicz, M.; Zaremba, W.; Abbeel, P. Sim-to-Real Transfer of Robotic Control with Dynamics Randomization. In Proceedings of the 2018 IEEE International Conference on Robotics and Automation (ICRA), Brisbane, Australia, 21–25 May 2018; pp. 3803–3810. [CrossRef]

149. Lee, J.; Hwangbo, J.; Wellhausen, L.; Koltun, V.; Hutter, M. Learning quadrupedal locomotion over challenging terrain. *Sci. Robot.* **2020**, *5*, eabc5986. [CrossRef]
150. Miki, T.; Lee, J.; Hwangbo, J.; Wellhausen, L.; Koltun, V.; Hutter, M. Learning robust perceptive locomotion for quadrupedal robots in the wild. *Sci. Robot.* **2022**, *7*, eabk2822. [CrossRef]
151. Kumar, A.; Fu, Z.; Pathak, D.; Malik, J. RMA: Rapid Motor Adaptation for Legged Robots. *arXiv* **2021**, arXiv:2107.04034. [CrossRef]
152. Gupta, A.; Savarese, S.; Ganguli, S.; Fei-Fei, L. Embodied intelligence via learning and evolution. *Nat. Commun.* **2021**, *12*, 5721. [CrossRef]
153. Clune, J.; Mouret, J.B.; Lipson, H. The evolutionary origins of modularity. *Proc. R. Soc. B Biol. Sci.* **2013**, *280*, 20122863. [CrossRef]
154. Laughlin, S.B.; Sejnowski, T.J. Communication in Neuronal Networks. *Science* **2003**, *301*, 1870–1874. [CrossRef]
155. Kirkpatrick, J.; Pascanu, R.; Rabinowitz, N.; Veness, J.; Desjardins, G.; Rusu, A.A.; Milan, K.; Quan, J.; Ramalho, T.; Grabska-Barwinska, A.; et al. Overcoming catastrophic forgetting in neural networks. *Proc. Natl. Acad. Sci. USA* **2017**, *114*, 3521–3526. [CrossRef]
156. Ijspeert, A.J. Central pattern generators for locomotion control in animals and robots: A review. *Neural Netw.* **2008**, *21*, 642–653. [CrossRef]
157. Di Carlo, J.; Wensing, P.M.; Katz, B.; Bledt, G.; Kim, S. Dynamic Locomotion in the MIT Cheetah 3 Through Convex Model-Predictive Control. In Proceedings of the 2018 IEEE/RSJ International Conference on Intelligent Robots and Systems (IROS), Madrid, Spain, 1–5 October 2018; pp. 1–9. [CrossRef]
158. Hochreiter, S.; Schmidhuber, J. Long Short-Term Memory. *Neural Comput.* **1997**, *9*, 1735–1780. [CrossRef]
159. Cho, K.; van Merriënboer, B.; Gulcehre, C.; Bahdanau, D.; Bougares, F.; Schwenk, H.; Bengio, Y. Learning Phrase Representations using RNN Encoder–Decoder for Statistical Machine Translation. In Proceedings of the 2014 Conference on Empirical Methods in Natural Language Processing (EMNLP), Doha, Qatar, 25–29 October 2014; pp. 1724–1734. [CrossRef]
160. Cully, A.; Clune, J.; Tarapore, D.; Mouret, J.B. Robots that can adapt like animals. *Nature* **2015**, *521*, 503–507. [CrossRef]
161. Jonas, E.; Kording, K.P. Could a Neuroscientist Understand a Microprocessor? *PLoS Comput. Biol.* **2017**, *13*, e1005268. [CrossRef]
162. Gerhard, S.; Andrade, I.; Fetter, R.D.; Cardona, A.; Schneider-Mizell, C.M. Conserved neural circuit structure across Drosophila larval development revealed by comparative connectomics. *eLife* **2017**, *6*, e29089. [CrossRef]
163. Abbott, L.F.; Bock, D.D.; Callaway, E.M.; Denk, W.; Dulac, C.; Fairhall, A.L.; Fiete, I.; Harris, K.M.; Helmstaedter, M.; Jain, V.; et al. The Mind of a Mouse. *Cell* **2020**, *182*, 1372–1376. [CrossRef]
164. White, J.G.; Southgate, E.; Thomson, J.N.; Brenner, S. The structure of the nervous system of the nematode Caenorhabditis elegans. *Philos. Trans. R. Soc. London. B Biol. Sci.* **1986**, *314*, 1–340. [CrossRef]
165. Cook, S.J.; Jarrell, T.A.; Brittin, C.A.; Wang, Y.; Bloniarz, A.E.; Yakovlev, M.A.; Nguyen, K.C.Q.; Tang, L.T.H.; Bayer, E.A.; Duerr, J.S.; et al. Whole-animal connectomes of both Caenorhabditis elegans sexes. *Nature* **2019**, *571*, 63–71. [CrossRef]
166. Witvliet, D.; Mulcahy, B.; Mitchell, J.K.; Meirovitch, Y.; Berger, D.R.; Wu, Y.; Liu, Y.; Koh, W.X.; Parvathala, R.; Holmyard, D.; et al. Connectomes across development reveal principles of brain maturation. *Nature* **2021**, *596*, 257–261. [CrossRef]
167. Szigeti, B.; Gleeson, P.; Vella, M.; Khayrulin, S.; Palyanov, A.; Hokanson, J.; Currie, M.; Cantarelli, M.; Idili, G.; Larson, S. OpenWorm: An open-science approach to modeling Caenorhabditis elegans. *Front. Comput. Neurosci.* **2014**, *8*, 137. [CrossRef]
168. Zhao, M.;Wang, N.; Jiang, X.; Ma, X.; Ma, H.; He, G.; Du, K.; Ma, L.; Huang, T. An integrative data-driven model simulating C. elegans brain, body and environment interactions. *Nat. Comput. Sci.* **2024**, *4*, 978–990. [CrossRef]
169. Ryan, K.; Lu, Z.; Meinertzhagen, I.A. The CNS connectome of a tadpole larva of *Ciona intestinalis* (L.) highlights sidedness in the brain of a chordate sibling. *eLife* **2016**, *5*, e16962. [CrossRef]
170. Hildebrand, D.G.C.; Cicconet, M.; Torres, R.M.; Choi, W.; Quan, T.M.; Moon, J.; Wetzel, A.W.; Champion, A.S.; Graham, B.J.; Randlett, O.; et al. Whole-brain serial-section electron microscopy in larval zebrafish. *Nature* **2017**, *545*, 345–349. [CrossRef]
171. The MICrONS Consortium. Functional connectomics spanning multiple areas of mouse visual cortex. *Nature* **2025**, *640*, 435–447. [CrossRef]
172. Shapson-Coe, A.; Januszewski, M.; Berger, D.R.; Pope, A.; Wu, Y.; Blakely, T.; Schalek, R.L.; Li, P.H.; Wang, S.; Maitin-Shepard, J.; et al. A petavoxel fragment of human cerebral cortex reconstructed at nanoscale resolution. *Science* **2024**, *384*, eadk4858. [CrossRef]
173. Aldarondo, D.; Merel, J.; Marshall, J.D.; Hasenclever, L.; Klibaite, U.; Gellis, A.; Tassa, Y.; Wayne, G.; Botvinick, M.; Ölveczky, B.P. A virtual rodent predicts the structure of neural activity across behaviours. *Nature* **2024**, *632*, 594–602. Correction in *Nature* **2025**, *645*, E1. [CrossRef]

Disclaimer/Publisher's Note: The statements, opinions and data contained in all publications are solely those of the individual author(s) and contributor(s) and not of MDPI and/or the editor(s). MDPI and/or the editor(s) disclaim responsibility for any injury to people or property resulting from any ideas, methods, instructions or products referred to in the content.